Bio-Design and Manufacturing (2025) 8:310–330
https://doi.org/10.1631/bdm.2400235

RESEARCH ARTICLE

Development of a multifunctional uniaxial bioreactor with real-time monitoring of culture conditions and tissue health

Adit Mehta[1] · Po-Feng Lee[1] · Eric Renteria[1,3] · Frank C. Marini[1] · Ji Hyun Kim[1] · Tracy Criswell[1] · Thomas D. Shupe[1] · Anthony Atala[1] · Metin N. Gurcan[2] · Shay Soker[1] · Joshua Hunsberger[3] · James J. Yoo[1] · Young Min Ju[1]

Received: 12 June 2024 / Accepted: 19 October 2024

Abstract

Bioreactors are used to dynamically condition engineered tissues to achieve the required degree of maturation before in vivo implantation. Integrating sensors and imaging capabilities into bioreactors can help us understand how the culture environment influences tissue maturation and growth. Additionally, this enables the monitoring of tissue constructs and provides critical information for quality control. This study aimed to develop a standardized, self-contained, uniaxial bioreactor module for the clinical manufacturing of tissue constructs; this system would benefit from unidirectional mechanical or electrical stimulation, or both. We achieved this goal by integrating stimulation and sensing components that provide an optimal culture environment and monitoring capabilities to improve tissue manufacturing. The uniaxial bioreactor module included integrated, user-friendly mechanical and electrical stimulations with force measurement to enhance the preconditioning of the engineered tissues. Also, a sensor loop and media exchange system were integrated to monitor the culture environment and cellular metabolites over time, and the camera system above the tissue construct enabled the macroscopic visualization of tissue maturation. Furthermore, the onboard media exchange system was programmed into the module to maintain aseptic culture conditions in the long term. Subsequently, using native skeletal muscle tissue and tissue-engineered skeletal muscle constructs, the performance of the uniaxial bioreactor module was validated for its application in preconditioning and enhancing tissue maturation.

Adit Mehta and Po-Feng Lee have contributed equally to this work.

✉ Young Min Ju
yju@wakehealth.edu

[1] Wake Forest Institute for Regenerative Medicine, Wake Forest School of Medicine, Winston-Salem, NC 27157, USA

[2] Center for Artificial Intelligence, Wake Forest School of Medicine, Winston-Salem, NC 27157, USA

[3] RegenMed Development Organization (ReMDO), Winston-Salem, NC 27106, USA

Graphical abstract

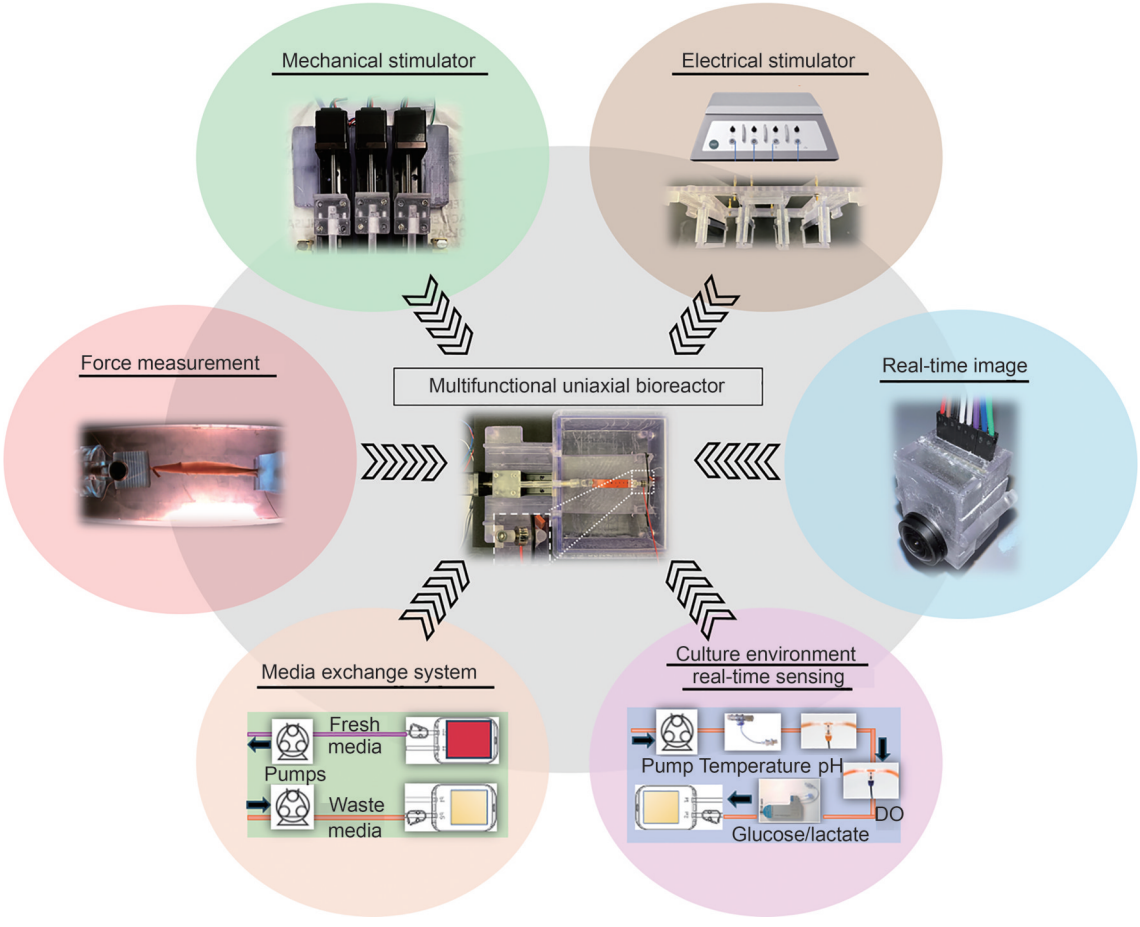

Keywords Bioreactor · Manufacturing · Monitoring sensors and automation · Regenerative medicine · Tissue engineering

1 Introduction

Traditionally, bioreactors have been used for in vitro cell expansion in a controlled biochemical growth environment [1]. Meanwhile, tissue bioreactors utilize cells applied to a two-dimensional (2D) or three-dimensional (3D) scaffold, reflecting the physical geometry and architecture of a native tissue [2, 3]. A tissue bioreactor provides an anchoring bracket for the engineered tissue, an environment conducive to cell differentiation and tissue maturation, and mechanical conditioning for the tissue. Generally, tissue engineering constructs do not initially maintain a degree of durability or function required for in vivo implantation; their maturation within a tunable bioreactor ensures their subsequent successful implantation [4].

For the effective manufacturing of engineered tissue constructs, the in vitro culture environment should closely mimic the in vivo tissue environment, including appropriate biochemical environment (soluble bioregulatory factors, pH, pO_2, etc.) and physical (electrical and mechanical force) stimuli [5–8]. Therefore, an optimal bioreactor should have material biocompatibility, mechanisms for physically stimulating tissues, an appropriate biochemical environment, biosensing capabilities, and sterility maintenance [4, 9, 10].

Functionalities can be added to a bioreactor by integrating additional components into it. Such integrated components are made from biocompatible materials. Most biocompatible materials, such as polymer resins, are difficult to use for prototyping in the laboratory; however, due to the advancement and reduced cost of additive manufacturing, bioreactor chambers or parts have been 3D-printed for research use [11, 12]. In addition, many polymer resins have been used and tested for their cytotoxicity [13–15].

In terms of choosing a model tissue for optimizing tissue bioreactors, engineered muscles represent an excellent choice [16]. Skeletal muscles, making up approximately

40% of the human body mass, are the primary mechanism for locomotion [17]. Although skeletal muscles can regenerate following mild or moderate injury, there is no effective treatment for significant muscle loss [18]. Thus, skeletal muscle is a major research focus of tissue engineering.

Bioreactors used for preconditioning and culturing engineered skeletal muscles consist of uniaxial stretching systems that expand the muscle construct through controllable static or cyclic stretching programs. The expansion is generally accomplished by affixing the muscle construct between a stationary and a moveable mount. The muscle construct is stretched using electro-mechanical devices, such as solenoids, stepper motors [19–25], electromagnets [26], pneumatic pumps [27], or syringe pumps [28]. Exercising tissue constructs by applying tensile forces to them facilitates myogenesis, enhances myotube formation [23], elevates force production [29], and increases cell viability, proliferation, and alignment. Uniaxial bioreactors are used for the engineering of soft tissues; they have a linear movement that generates unidirectional forces, such as those generated by muscles [19–21], ligaments, and tendons [30, 31]. Most bioreactors use a single large motor to generate mechanical forces; therefore, they cannot provide multiple strain ratios for stimulating different constructs simultaneously. As a result, it has not been possible to conduct studies that compare different strain ratios or rates across multiple constructs within a single bioreactor.

Another common component incorporated into skeletal muscle tissue bioreactors is an electrical stimulator. Electrode pairs immersed in the media within the cell culture chamber provide the desired stimulation pattern in commercial or improvised systems [21, 32, 33]. For that effect, several electrode materials have been used to stimulate the tissue constructs [34]. For example, carbon electrodes are an excellent option for delivering electrical stimulation, as they are non-toxic and cost-effective, have superior charge application characteristics and high corrosion resistance, and do not leach materials into the media during high-current electrochemical stimulations over long periods [35]. Electrical stimulation to the engineered constructs increases cell proliferation, improves cell alignment in fibers, and increases tissue contractility [36]. Electrical stimulation is also used to assess the functionality of engineered muscle constructs by stimulating them with high-frequency pulses to measure the peak twitch contractile forces they generate. Twitch forces, which are measured by a force transducer, are often used to measure the contractility of engineered skeletal muscles [37–40].

Additionally, a force-sensing component of the bioreactor is essential for determining the maturation of muscle tissue over time [41]. Previously, this was achieved with optical deflection measurement, followed by calculation of contractile force output [42]. More recently, bioreactors have incorporated direct [20] or indirect methods [43, 44] to quantify contractile forces. Since the force generated by the engineered tissue is small (in micro-newtons) [38], the system needs to be sufficiently sensitive to provide accurate measurements of force generation with maximum noise-free resolution. In addition, multifunctional bioreactors require validation of their integrated components to ensure comprehensive and coordinated tissue maturation [45].

Tissue constructs mature within bioreactors over a period of 10 to 28 d. Consequently, it is necessary to replace the culture medium periodically to replenish the crucial nutrients that support cellular growth, such as glucose, and to eliminate the accumulated waste substances, including lactate, to maintain a consistent pH. In a typical cell culture, the medium is changed at fixed intervals to maintain consistent culture conditions [46]. Since bioreactor systems are designed to be semi-closed or fully closed systems to prevent contamination of the engineered constructs, regular media changes present a cumbersome challenge. Therefore, integrating a real-time media monitoring system would be beneficial for ensuring proper media changes when needed.

In this study, we described the development and validation of a multifunctional uniaxial bioreactor that can be independently configured for dynamic culturing protocols using mechanical and electrical stimulation. In addition, using native skeletal and engineered muscle tissue constructs, we demonstrated real-time feedback for actuator movement, generation of electrical stimulation pulses, force generation of the engineered construct, macro-imaging, and sensing of the tissue environments.

We have designed, developed, or integrated several components. First, we designed and developed a mechanical subsystem with three linear actuators, which facilitated the programming of separate strain ratios, allowing for three different constructs to be cultured simultaneously. Second, we designed and developed an electrical stimulation subsystem that integrated carbon electrode pairs into each culture lane to receive pulse input from any commercial stimulator. Third, we integrated force sensors into each culture lane to read mechanical stretch forces and isometric contraction forces. Fourth, we integrated commercially available media sensors for pH, dissolved oxygen, temperature, glucose, and lactate. Fifth, we designed a system that had a translucent port for imaging the tissue via an external monitoring camera. Finally, we developed a fixed-volume media exchange system, which could be triggered manually or timed via a system clock and relays.

By combining these capabilities, we have created a user-friendly and standardized culturing system that reduces the risk of contamination by automating essential tasks throughout the culturing period and utilizes several subsystems for the effective culturing of tissue constructs that require uniaxial durability or force generation, or both.

2 Materials and methods

2.1 Bioreactor design and fabrication

2.1.1 3D-printed bioreactor housing

All components for the complete system assembly were designed using the SolidWorks 3D CAD (Hawk Ridge Systems, Mountain View, USA), exported in the stereolithography (SLA) format, 3D-printed with Biomed Clear Resin (Formlabs, Somerville, USA; a commercial biocompatible photopolymer resin) using a Formlabs SLA desktop 3D printer (Form 3B, Formlabs, Somerville, USA), and washed/cured according to the manufacturer's guidelines.

The bioreactor culture box had three moveable shafts connected to the actuators via three holes in the rear wall, limiting the effective maximum volume to 600 mL. In addition, 250 mL of media were needed to submerge the tissues in culturing experiments when anchored to tissue grippers. A 9.5-mm-thick polycarbonate sheet with ultra-violet (UV)/scratch resistance was cut into two trays to place the bioreactor module and the sensor loop on the top using 3D-printed snap-fit connectors. The module was designed to fit inside a compact cell culture incubator (MCO-50AIC, PHCbi, Wood Dale, IL, USA), which maintained a consistent temperature at 37 °C and CO_2 content at 5%.

Due to the availability of digital communication ports, Arduino ATmega2560 microcontrollers (Arduino, Monza, Italy) were used as the main microcontroller system. All wiring was polyvinyl chloride (PVC)-insulated copper conductors.

2.1.2 Integration of the mechanical stimulator

Individual mechanical stimulation patterns in each lane of the bioreactor were generated by placing three compact standard NEMA 11 stepper motor chassis with ball-screw mechanisms (1-mm pitch, 200 steps/revolution, and 1.8° step angle) and 1 kg maximum load ratings (ASIN# B087NMCGPV, Amazon.com, Bellevue, WA, USA) inside the 3D-printed actuator housing, loading with encoders on the ends, and fixing to the base with M3 screws (Fig. 1a).

In addition, three commercially available evaluation boards (EasyDriver, Sparkfun Electronics, Niwot, CO, USA) with a motor driver (A3967, Allegro Microsystems, Manchester, NH, USA) were used to run the step-motors, provide digitally programmable controls for the movement profile and microstepping resolution, and provide a step pulsing protocol capable of microstepping up to 1600 steps per revolution.

Based on the motor ratings, the span screw on the boards was used to tune the current limit to prevent the motors from overheating. The motors, rated at 600 mA, were safely paired with a driver chip of a maximum of 750 mA of current through the motor.

A variable resolution absolute encoder (CUI Devices, Lake Oswego, OR, USA), with up to 4096 pulses/mm, was fixed to the 3D-printed element of each motor to measure

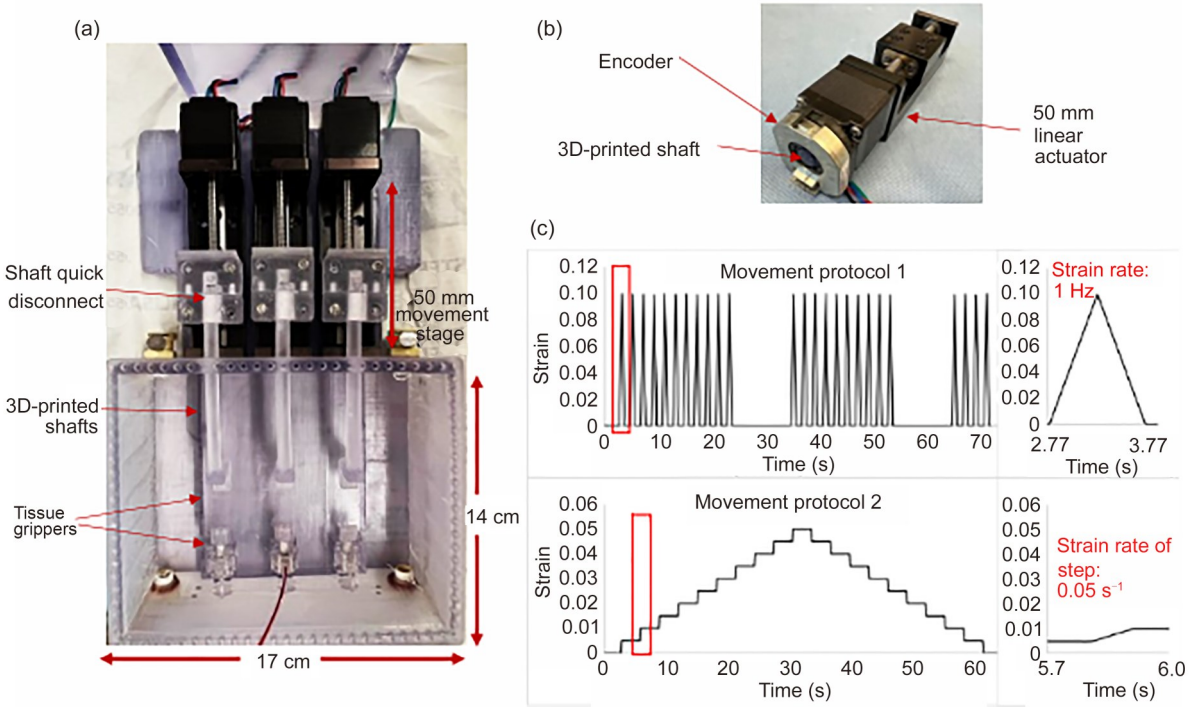

Fig. 1 Mechanical stimulation system. (a) Three individually configurable stretch systems were designed using three stepper motors with ball-screw guides. (b) Integration of a movement encoder. (c) Two movement protocols and their respective strain rates over time for cyclic strain and stepwise strain, as read by the encoder

the movement in steps and to record and verify the strain, strain rates, and protocol timings in real time during the culturing period (Fig. 1b). Based on the resolution needed and the microstepping mode used, the encoder's internal resolution of pulses per revolution could be increased or decreased.

The motor software used various parameters, such as the length of the tissue construct and the maximum percentage strain, to generate the strain amplitude. Also, the system provided a mechanical stretch of at least 10% to a tissue of up to 4 cm in length with a maximum actuator speed locked at 20 mm/s.

Two protocols were generated to validate the complete system (Fig. 1c). The first protocol was a cyclic strain with operational inputs, such as frequency (Hz), to define the speed and train time to calculate the number of stretch cycles internally rounded to the nearest integer and wait time between two training cycles. The second protocol was a stepwise strain with a tunable step size as a percentage of the original length and adjustable rest time between the steps to generate a stress–relaxation testing system [47]. Finally, a program was developed to increase or decrease the distance between the anchors for correct pretensioning.

2.1.3 Integration of the electrical stimulator

To provide electrical stimulation for tissue maturation or muscle contractile force generation, we designed three pairs of positive and negative male mini-banana connectors attached to the lid to transmit electrical stimulus pulses individually to parallel carbon plates inserted under the lid via platinum wires (Fig. 2a). The same polarity electrodes were placed next to each other to minimize the cross-interference of the fields [48].

The two carbon plate electrodes were kept 3 cm apart and immersed to a depth of 1.5 cm in the culture media when placed inside the culture chamber. The carbon electrodes were detachable and could be removed when not in use. A four-channel electrical stimulator (DMT, Ann Arbor, MI, USA), with banana cables connected to three pairs of connectors on the lid, was used to stimulate the muscle tissues. MyoPulse software (DMT, Ann Arbor, MI, USA) was used to control the stimulator functions, including pulse width, frequency, amplitude, and train parameter protocols, and could be triggered to start the channels individually or collectively using the microcontroller of the bioreactor. The digital output of the microcontroller was used as a trigger signal received through the rear panel of the stimulator.

The pulse characteristics were verified by connecting the fourth channel of the stimulator to a digital oscilloscope (PicoScope, Pico Technology, UK) (Fig. 2b). Continuity testing of the electrode circuit demonstrated a closed circuit when placed in the media, and the current output was read through the voltage drop measured across a 0.01% accuracy resistor, which varied linearly with the stimulator voltage [35]. Biphasic pulses were delivered through electrode pairs

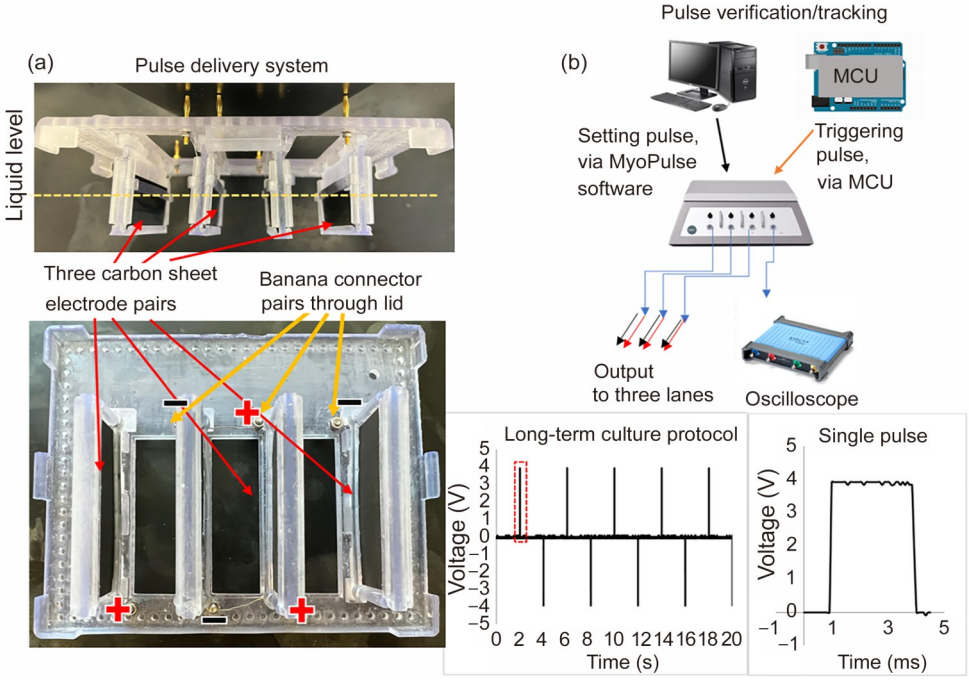

Fig. 2 Electrical stimulation system. (a) Three pairs of carbon sheet electrodes are held in spacers from the lid. The transfer of pulses from a pulse generator to the submerged electrode is simplified with the use of gold-plated mini banana connector pairs on the lid, with pairs inserted as marked by "+" and "−". (b) Integration of a DMT four-channel stimulator with simultaneous verification of the set pulse train characteristics using the fourth channel; long-term culture protocol as captured by the digital oscilloscope. MCU: microcontroller unit

placed parallel to the constructs [49]. Due to the limitations of the stimulator, a constant voltage output at a maximum of 30 V, or a maximum field strength of ±10 V/cm, could be applied across each lane simultaneously.

2.1.4 Integration of the force sensor

Three stainless steel uniaxial force sensors (Customized LCM100, FUTEK, USA) with waterproof and corrosion resistance properties were integrated into the system (Fig. 3a). The in-line compression and tension sensors had M3 male thread mounts at both ends. The body was locked inside a 3D-printed shell to minimize fluid contact with the cable, and one of the M3 threads was mounted to the removable base plate inside the culture chamber. The tissue gripper was screw-mounted to the other M3 thread at the end of the sensor. Then, the output was fed to a digital gain amplifier with a high signal-to-noise ratio (USB520, FUTEK, USA) and to the calibration and measurement software (SENSIT, FUTEK, USA).

The USB520 amplifier allowed for a 15-point (or lower) calibration program to fine-tune the output for small force readings, along with natural zero compensation, before putting the sensor in the shell. Then, two sets of calibrations were performed for the small and large force ranges, separately. For each, the base plate mounted with a force sensor was temporarily held vertically within a custom vise to hang standard weights of 1–5 g for stepwise calibration of up to 100 g. For calibration of small force measurements, small calibration steps were achieved by adding small volumes of water with a micropipette (PIPETMAN G, Gilson Incorporated, Middleton, WI, USA).

The force-sensing resolution was defined by a small-range calibration at a 100 μN step. The calibration result was saved as a profile in the internal memory of the digital amplifier. This practice would ensure accurate readings when the results were tested against known standard weights and pipetted water droplets. The theoretical resolution of

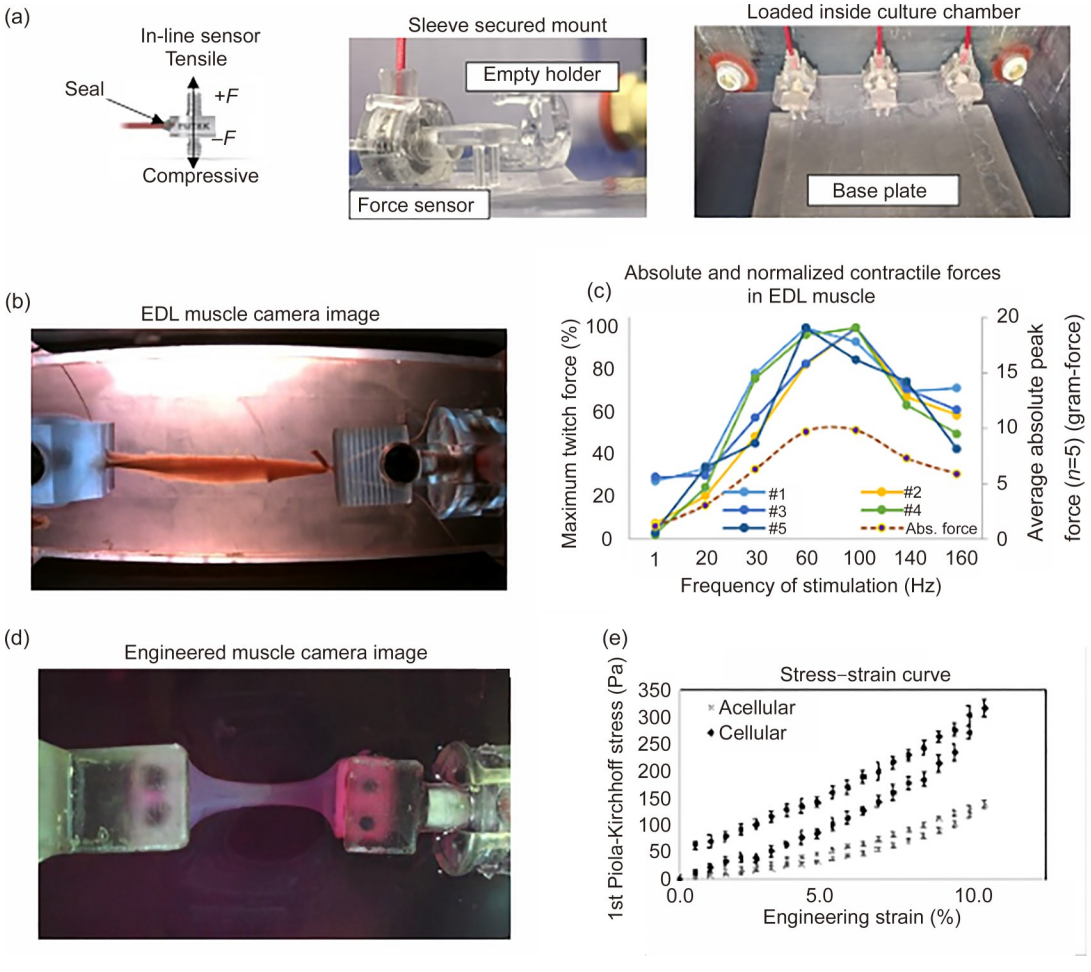

Fig. 3 Incorporation of force sensor. (a) A miniaturized submersible in-line sensor was used to measure the force in each lane. Setup with fresh rat EDL muscle anchored at tendons inside the bioreactor (b) and average peak force and percentage of maximum peak force per muscle, recorded at incremental frequency of stimulation (c). Setup with a hydrated fibrin gel scaffold (d) and the corresponding 1st Piola-Kirchhoff stress vs. strain graph of cellular and acellular scaffolds (e). EDL: extensor digitorum longus

our setup was calculated from the maximum capacity or range of the force sensor divided by the bit resolution of the analog-to-digital converter (ADC), yielding 0.53 μN for a 24-bit ADC. We assumed a water density of 1 g/mL to calculate the force. The force sensor amplifier could save four separate calibration curves in the electrically erasable programmable read-only memory (EEPROM) that could be easily accessed and selected through the software. After each sensor was calibrated, the base plate was fixed on the bottom of the bioreactor chamber.

2.1.5 Integration of the sensor loop system

Cellular metabolites and the general condition of the environment inside the bioreactor were monitored by developing a sensor loop that contained several single-use flow-through sensors, which were connected to the bioreactor through a perfusion loop system using a peristaltic pump (P625; Instech Labs, Plymouth Meeting, PA, USA) (Fig. 4a). All tubing used was flexible processed tubing (C-FLEX Clear Process tubing; Masterflex, Vernon Hills, IL, USA) with a 1/16-inch inner diameter, and a PharMed BPT tubing (PharMed Pump Tubing/P625; Instech Labs, Plymouth Meeting, PA, USA) was used as the pump tubing. The flow-through sensor ports were coupled to the tubing using polypropylene hose barbs, Luer-locks, and valved quick disconnect body and insert pairs (Colder Products Company, St. Paul, MN, USA). When the perfusion ports of the chamber were panel-mounted for quick disconnection, the tubing side of the inserts had a 1/8-inch flow diameter. Lastly, four media sensors (for glucose, lactate, dissolved oxygen (DO), pH, and temperature monitoring) were connected in a perfusion loop.

- Glucose-and-lactate sensor: A biosensor transmitter (SIX-OEM; IST-AG, Toggenburg, Switzerland) with an adapter for single-use sensors was connected to the microcontroller via a universal asynchronous receiver transmitter to register readings from the glucose-and-lactate dual sensor (BLV.5, Jobst, IST-AG, Germany).
- pH and DO sensors: Two fiber optic cable lines were connected to the pH and DO sensors (Scientific Bioprocessing, USA), and data were saved via the USB software (ID.Data-Hub, Scientific Bioprocessing, USA) using a Python library for integration purposes. The pH and DO sensors were pre-calibrated and came with a calibration code that could be manually entered through the software.
- Temperature sensor: A single-use temperature sensor (Pendotech, Princeton, NJ, USA) was placed in line with the pH and DO sensors. The temperature sensor was connected to a simple voltage divider circuit to read the change in resistance in the thermistor-based flow. Data were saved via analog input to the microcontroller.

The sensing system was assembled on a polycarbonate tray with all the components mounted on dedicated 3D-printed holders. The bioreactor perfusion system (Fig. 4a) had the flow line and the normally open and normally closed (NO & NC) lines of the three-way pinch valves, which could switch between the sampling solutions for the glucose-and-lactate sensor. One end of the system had tubing with a quick disconnect connector linking it to the bioreactor (Fig. 4b). The tray held Dulbecco's phosphate-buffered saline (PBS) buffer (DPBS; Cytiva, Marlborough, MA, USA) and a glucose/lactate calibration solution, which could be a commercial standard (2747 Standard; YSI, Yellow Springs, OH, USA) or serum-supplemented media used in the experiment. These were loaded into two different bags (100 mL 2D Labtainer; Thermo Fisher Scientific, Waltham, MA, USA) for intermittent washing and calibration of the glucose-and-lactate sensor. Two Omnifit polyether ether ketone (PEEK), 10 μm polytetrafluoroethylene (PTFE) low-flow bubble traps (Diba Industries Inc., Danbury, CT, USA) were fitted to prevent bubbles from entering the system from these bags. The sensor loop system was set to withdraw a fixed-volume sample of 200 uL from a desired source. A small peristaltic pump placed at the end of the one-way sensor loop could be switched to collect a sample from a PBS buffer solution bag, a glucose/lactate calibration solution bag, a bioreactor media bag, or an incubator air supply via three three-way solenoid pinch valves, which were labeled PV1 to PV3 and activated by a microcontroller using a standard relay circuit (Fig. 4a).

Heat generation during prolonged operations was avoided by placing a hit-and-hold circuit CoolCube (Cole-Parmer, Vernon Hills, IL, USA) before the valves. Different liquids were isolated without mixing using PV1 at the beginning of the sensor loop to pull in the incubator air to separate the different fluids going to the sensor. The flow rate was set to 1.6 mL/min without exceeding the limit of the glucose-and-lactate sensor, which had the smallest flow rate limit among all the sensors in the loop.

These fluids were received by the glucose-and-lactate sensor, placed at-line, followed immediately by an ultrasonic liquid-bubble sensor (AE301, Panasonic Industrial Automation, Newark, NJ, USA) before reaching the peristaltic pump. To avoid timing errors in fluid sampling caused by differences in tubing length between experiments, the no-contact liquid-bubble sensor was used to help automate fluid movement in the sensor loop by non-invasively detecting the presence and absence of liquid in the latched tubing. The tubing downstream from the pump was connected to a plastic waste container.

Altogether, we designed the system for semi-continuous monitoring to minimize the exposure of the glucose-and-lactate sensor in highly concentrated glucose media, which could degrade the sensor performance during long-term

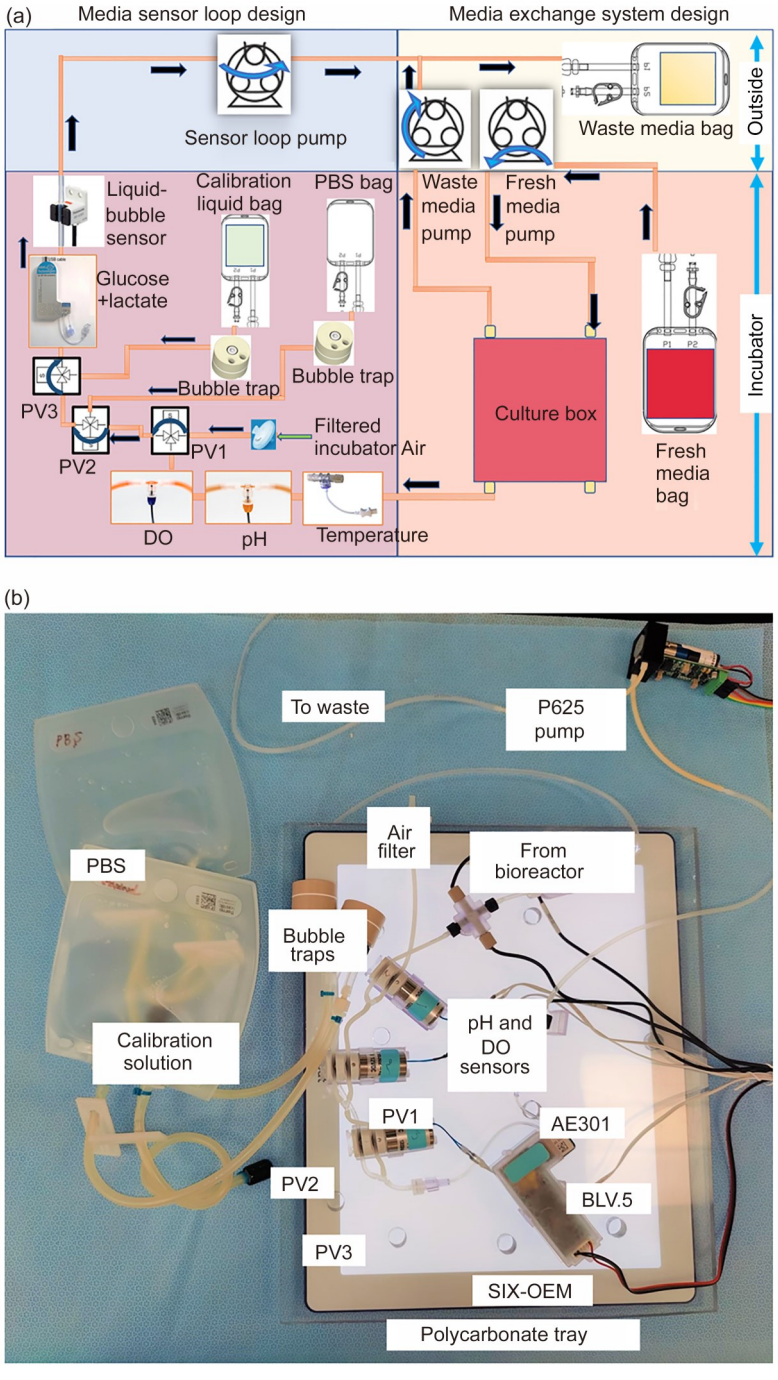

Fig. 4 Design of sensor loop and media exchange system. (a) The sensor loop is designed to automate the fluid movement for media sensing, where sensors are exposed to media from the culture box, PBS buffer, or glucose/lactate calibration solution by controlling the sensor loop pump and three three-way solenoid pinch valves (PV1–PV3). The media exchange system has two pumps that can be manually turned on/off for media fill and emptying purposes. (b) Final physical assembly of the sensor loop tray with three-dimensionally printed parts. PBS: phosphate-buffered saline; DO: dissolved oxygen

operations [50]. A buffer (PBS) wash system was added to rinse the residual media from the sensor loop tubing. A calibration solution containing fresh, complete media with known glucose and lactate concentrations was sampled to calibrate the sensors after a user-defined number of rounds. For accuracy in automatic calibration, the initial glucose-and-lactate content in the complete media was measured using the CEDEX Bioanalyzer (Roche Diagnostics, Switzerland). The system autonomously selects the sample sources, i.e., the bioreactor media, PBS washing buffer, or calibration solution, with air gaps to prevent liquid collapse. It recorded glucose-and-lactate concentrations by pre-defining variables,

such as measurement intervals, counts before re-calibration, known concentrations in the calibration solution, plateau time, and data averaging duration before file recording.

Media withdrawal from the bioreactor for sensing was optimized by making the liquid-bubble sensor's ON and OFF outputs function as triggers to start and stop the pump and switch relays running the solenoid valves. Rather than relying on the timer, the perfusion system could define functions, such as "wait till ON" or "wait till OFF," to automate the movement of the sampled fluids. The appropriate stoppage of each fluid at the required location and the measurement and recording thereof within the perfusion loop were programmed based on the maximum time for the individual sensors to reach 95% of the final response value. This time was examined by studying the reaction time by exposure to different analyte solutions for each sensor.

The ability of this system to consistently provide accurate repeated readings was tested by performing a three-day sensor monitoring study with media without cells, and data were collected every 3 s for 72 h (Fig. S1 in the supplementary information). For calibration solutions, 10 mmol/L glucose and 5 mmol/L lactate solutions were used, and high-glucose Dulbecco's modified Eagle medium (DMEM; 25 mmol/L glucose and 0 mmol/L lactate; Sigma-Aldrich, St. Louis, MO, USA) was used in the bioreactor at 37 °C and 5% CO_2.

Although the calibration solution was sampled each time, the calibration of the sensors was only performed at the beginning of the experiment to check for changes in the raw reading of the calibration solution over time, which indicated potential sensor degradation. Every hour, the first observed plateau represented the known glucose and lactate concentrations in the calibration solution. The second plateau measured glucose and lactate from the bioreactor media. The first sensor exposure was to air, which showed no reading (yellow), followed by a PBS wash (blue), air (yellow), and the calibration solution (green). This cycle was then repeated to test the bioreactor media (Fig. S1 in the supplementary information). The data described above were plotted by matching the peaks in the first 8 min of the hourly exposures using a custom Python code. The peaks matched at the zero-point were shown to overlap (Fig. S1 in the supplementary information).

The amount of time the sensors took to return to baseline between consecutive readings was determined using a predetermined concentration of solute, followed by air (observed as sudden peak to saturation), PBS (fall to baseline), and air before the same concentration of solute was again added (Fig. S1 in the supplementary information).

Next, 2D-cultured C2C12 skeletal muscle cells were used to further test the functionality of the sensor loop system by measuring the culture-induced media changes.

The last component to be assembled was the media exchange system, which had two peristaltic pumps (KDM-OCM, Kamoer, China) for media aspiration and replacement, separately (Fig. S2 in the supplementary information). The first pump connected the bioreactor housing to a media waste bag (2000 mL 2D Labtainer, Thermo Fisher Scientific) for removing old media, and the second pump was for transferring media from the fresh media bag (250 mL 2D Labtainer, Thermo Fisher Scientific) to the culture chamber. The waste media bag and the media exchange pumps were placed outside the incubator with the tubing passed through the rear access hole of the incubator. Both pumps were controlled using physical ON/OFF buttons, calibrated for flow rates, and set to 100 mL/min for withdrawal and 40 mL/min for refill. The refill rate was selected for a fast media exchange without disturbing the tissue-engineered construct.

2.1.6 Integration of the imaging system

The lid of the bioreactor system was designed with three rectangular ports, and a glass microscope slide was secured into each for imaging the construct in real time. The USB-16MP (Arducam, China) low-light camera assembly consisted of a 1/2.8-inch 16MP IMX298 image sensor secured within a 3D-printed case. The entire assembly was placed on top of the culture chamber lid facing the culture lanes, allowing for imaging through the glass slide window. An adjustable light source was positioned below the bioreactor tray for capturing images and videos.

2.2 Functional validation of the uniaxial bioreactor system

2.2.1 Native rat muscle tissue model

Freshly excised rat extensor digitorum longus (EDL) muscle was used in the system validation studies using a strategy similar to force-sensing studies with an organ bath. Fresh EDL muscles were harvested from Wistar rats weighing approximately 400 g following euthanasia and stored in Ringer's solution (0.125 mol/L NaCl, 1.5 mmol/L $CaCl_2$ dihydrate, 5 mmol/L KCl, and 0.8 mmol/L $NaPO_4$ dibasic) at 4 °C. In the force-sensing validation experiments, the tendons at each end of the EDL muscle were aseptically secured to tissue grippers in the culture chamber, with one end affixed to the force sensor and the other attached to the linear actuator. The muscles were cultured in high-glucose DMEM with 2% horse serum. The muscles (n=5) were electrically stimulated under isometric conditions at discrete frequencies of 1, 20, 30, 60, 100, 140, and 160 Hz, and peak forces for each frequency were plotted for each muscle. For each group, 1 min of force measurement was recorded, and data for the peak force were calculated from the region of train stimulation by the averaged peak-to-peak difference. To normalize the contractile forces to account

for the natural variations among muscles and differences in harvest to testing time between the muscles, we assumed the peak force for that muscle to be 100% at whichever frequency that might have occurred to visualize the trend of the generated contractile force. We further collected video records of muscle contractions, such as those at 1 Hz (Video S1 in the supplementary information).

For tissue survival testing, newly excised rat EDL muscles were loaded into two separate bioreactors for electrical and mechanical stimulation, respectively. The EDL tissue specimens were collected from the rats euthanized under an existing Wake Forest University Institutional Animal Care and Use Committee (IACUC) approved protocol (A20-147). The mechanical stimulation protocol for the muscles consisted of a 5-min stimulation and a 55-min rest per hour over 3 d. Each stimulation period consisted of 10% cyclic stretch for 20 s at a strain rate of 1 Hz and 1 s rest in between each stretch, making an effective frequency of 0.5 Hz, similar to other studies done on skeletal muscle tissues [51, 52]. The electrical stimulation protocol consisted of 3 V/cm electrical pulses with a pulse width of 0.3 ms, a frequency of 70 Hz, and a pulse train period of 400 ms; this was repeated every 1.6 min for 3 d. Three pieces of freshly excised EDL muscle tissue were used as the fresh control group (Fresh). The static control (Control) muscles were placed into the bioreactor culture chamber without anchoring to the tissue grippers and left to float freely. After 3 d of culture, all muscles were collected and fixed with 10% neutral buffered formalin for processing and histological assay. After fixation, the muscles were paraffin-embedded, sectioned, and stained with hematoxylin and eosin (H&E) and Masson's trichrome. All sections were imaged using an optical upright microscope (BX-63, Olympus Life Science Solutions, Japan), and the images were quantified using ImageJ (NIH, Bethesda, MD, USA).

2.2.2 Tissue-engineered muscle construct model

C2C12 myoblast cells (American Type Culture Collection, Manassas, VA, USA) at Passage 6 or lower were used, cultured in a growth medium (low-glucose DMEM and 10% fetal bovine serum), to generate tissue-engineered skeletal muscles. The engineered muscle mold was designed using SolidWorks (Hawk Ridge Systems, Mountainview, CA, USA) and manufactured using a Form 3B 3D printer (Formlabs, Somerville, MA). The 3D-printed mold consisted of a base piece with anchoring pillars, a middle well element, and a top lid element (Fig. S3 in the supplementary information).

The engineered muscle was fabricated in the mold using a gel-based casting method. Briefly, the base and middle well pieces were assembled, and two 4 mm×8 mm polyethylene cutouts with pore sizes of 45–90 μm (SP Bel-Art Fritware, Warminster, PA, USA) were inserted through the pillars of the base element, followed by the addition of a fibrin/cell mixture with a cell density of 5×10^6 cells/mL in DMEM supplemented with 10 mg/mL fibrinogen, 10 U/mL thrombin, 0.08 mg/mL aprotinin, and 50 ng/mL insulin growth factor. The engineered muscle constructs were polymerized after adding thrombin to the fibrinogen/cell mixture in the molds inside a culture hood for 10 min before equilibration inside the incubator for another 50 min. After the gel was polymerized, 1 mL of growth medium was added to the molds before covering them with the lid. The gels were cultured for 2 d.

A total of nine pieces of C2C12-encapsulated engineered muscle were produced and assigned to three separate groups: the Control group (n=3), the mechanical stimulation (MS) group (n=3), and the electrical stimulation (ES) group (n=3). The control samples were placed inside the bioreactor but did not receive any stimulation. The stimulation settings of the MS and ES groups were the same as those for the three-day culturing experiment with rat EDL muscles. All groups were cultured inside the bioreactors for 14 d in differentiation media.

2.2.3 Tissue evaluation

The tissue mechanical properties of the scaffolds, in the presence or absence of cells, were determined using a stepwise strain protocol with a maximum of 10% strain to avoid plastic damage and tissue deformation. The 1st Piola-Kirchhoff stress (1-PK stress) was calculated by assuming a constant cross-section measurement from the initial mold design. The cross-sectional area (CSA) could be input into the system from the mold design, displaying 1-PK stresses in real time. Video recording for this evaluation is available for cellular grafts (Video S2 in the supplementary information).

The morphology of the tissue-engineered muscles was evaluated after a 14-day differentiation period. Tissue transparency was observed by placing the engineered muscles on a liquid crystal display (LCD) panel (LightPad-Go; Cricut, South Jordan, UT, USA) with the same backlit light density. Then, the engineered muscles were loaded into the base element of the mold with the two sets of pillars to observe their lengths after stimulation compared with their original lengths.

After macrostructural evaluation, all engineered muscles were processed for histology and immunostaining. Briefly, the samples were fixed with 10% neutral buffered formalin at room temperature for 1 h and washed with PBS. The central region of each fixed sample, approximately 5 mm in length, was excised for immunostaining. Then, the samples were treated with 0.2% Triton-X in PBS for 5 min, rinsed with PBS, and blocked with 1× protein block (AB126587; Abcam, UK) for 20 min. Next, the samples were incubated

with primary antibodies against myosin (MF20; Invitrogen Antibodies, Carlsbad, CA, USA) and desmin (AB32362; Abcam, UK), separately, at 4 °C overnight. On the next day, the samples were washed with PBS and incubated with a secondary goat anti-mouse IgG antibody conjugated with Alexa Fluor 488 (A-11001; Invitrogen) or a goat anti-rabbit IgG antibody conjugated with Alexa Fluor 568 (A-11036; Invitrogen) at room temperature for 30 min. After a final wash with PBS, the samples were mounted in an anti-fade mounting medium with 4',6-diamidino-2-phenylindole (DAPI; Vector Laboratories, Newark, CA, USA) and imaged using confocal microscopy. ImageJ was used to quantify the myotube length and width and nuclei per myotube. The fusion index was defined as the percentage of the nuclei fused into myotubes per total number of nuclei in a field of view.

2.3 Statistical analysis

Students' *t*-test was used to establish the significance of differences in the quantification results for the EDL and engineered muscle experiments. A *p*-value of less than 0.05 was considered significant.

3 Results

3.1 Bioreactor system assembly

Two sets of trays were designed for the bioreactor and sensing modules of the full system (Fig. 5a) with their inputs/outputs and controllers (Fig. 5b). The bioreactor tray, which accommodated the bioreactor culture chamber, was successfully integrated with the mechanical stimulation system, force sensors, and electrical stimulation electrodes. The sensor module tray included the pinch valves, media sensors, biosensor transmitter, liquid-bubble sensor, and fluid bags containing PBS and the calibration solution. The materials used in all system parts were selected to be microbe-resistant and non-leaching. In the end, the two trays were found simple to assemble in a sterile hood and easy to handle for assembly within the tissue culture incubator.

3.2 Mechanical and electrical stimulation

A mechanical stimulation subsystem was designed with real-time feedback-capable movement that could be defined via customized protocols. The system provided high-resolution steps and an encoder to acquire accurate movement data. The motor driver allowed for real-time access to changing the microstep function and sleep and step profiles without changing the physical setup.

Two stimulation profiles were generated to test the cyclic stimulation and material properties. In addition, data were collected every 10 min from the encoder, according to the two tissue stimulation protocols (Fig. 1c). The feedback curves for the culture and stepwise strain protocols showed no observed error in the stepper's movement, as defined in our studies.

Carbon electrodes are an excellent option for electrical stimulation delivery because they are biocompatible and do not leak cytotoxic byproducts during high-level electrical stimulation over long culturing periods [53, 54]. The electrodes were placed parallel to the long axis on both sides of the muscle tissue, creating an electrical field

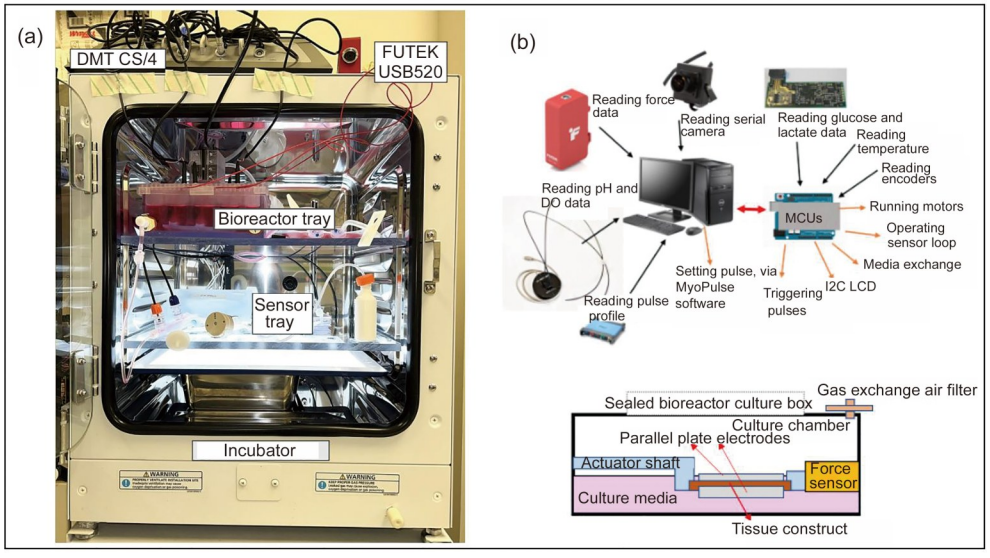

Fig. 5 Fully assembled uniaxial bioreactor system with operations. (a) Complete assembly inside the incubator for the bioreactor and sensor loop system. (b) Schematic diagram of the developed bioreactor's subsystem operations running together with MCUs and the computer; side view of the internals of the culture chamber. MCUs: microcontroller units; DO: dissolved oxygen; I2C: inter-integrated circuit; LCD: liquid crystal display

perpendicular to the construct [49]. The parallel plate electrode configuration allowed for the generation of a straight field line in 3D tissues, performing better than rod-shaped electrodes. The capacitive field aligned the cells perpendicularly to the field in the direction of the long axis. The voltage and current were tested using the system placed in the media. The pulse protocol was used for the culturing and excitation of the EDL muscle for contractile activity testing (Fig. 2b). The availability of more than one stimulation channel enabled the simultaneous study of multiple tissues in the bioreactor. The ability of the microcontroller to start the defined pulse protocol enabled studies that had in-phase and out-of-phase co-stimulation from electrical stimulators, such as those used in this study [55].

The calibration of the force sensor in the vertical orientation was performed inside an incubator at 37 °C. The maximum force measurement of the sensor was 1 kg-force or around 9.8 N. Owing to noise, the low-force calibration profile ensured a resolution of 50 μN. The force sensor integrated into the bioreactor could withstand multiple cycles of sterilization and long-term use submersed in the tissue culture media.

3.3 Automated sampling, calibration, and sensor loop system

An automated sampling and sensor calibration system was developed to monitor the metabolic activity of the cultured tissues and the general culturing environment within the bioreactor. The initial glucose and lactate contents, as measured by the Bioanalyzer, were 23.42 and 1.89 mmol/L, respectively, which could be attributed to the addition of 10% serum.

A 2-min period was determined to be required for reaching a final, stable measurement from the beginning to the time of reaching the plateau of interest (Fig. S1 in the supplementary information). The time required was 20 s for the temperature sensor and 10 min for the pH and DO sensors. Thus, the sensor loop was designed to have a minimum measurement cycle of 11 min. The system automatically recalculated the calibration gains for the output by automatically sampling the calibration solution before each measurement, thereby providing accurate readings even as the performance of the sensors degraded over time.

By design, the sensor system could read temperatures between 20 and 45 °C due to the resistor configuration used to increase sensitivity in the range of interest. In addition, the measurement of glucose and lactate concentrations ranged within 0–25 and 0–12.5 mmol/L, respectively. Moreover, the range of the pH sensor was limited to 6–8, as cell cultures were almost exclusively maintained within this range. Additionally, the range of DO that could be monitored was 0%–21%. Lastly, the percentage error range of the sensor hardware, as listed by their manufacturers, was within the scope of our experiments.

Finally, the five sensors in the sensor loop system successfully monitored the dynamic culture environment of the 2D-cultured C2C12 cells, validating the system's intended purpose of supporting clinical manufacturing quality control (Fig. 6). A media change was performed at 40 h; afterward, the glucose concentration and pH increased, the lactate concentration decreased, and the temperature and DO levels did not change.

3.4 Bioreactor system validation using native rat muscle tissues

The pulse protocol was used for the culturing and stimulation of EDL muscles for contractile activity investigation (Fig. 2b). Since our system had a fixed width between the electrodes, the force output for the five muscle samples tested showed an incremental peak force relative to the increasing frequency. The absolute forces at each frequency and the normalized average percentage peak force of these values for each frequency were measured (Table 1). For most muscles, the peak force dropped after 100 Hz (Fig. 3c). The resolution of the force readings was sufficient to determine the twitch and tetanic contractions at different stimulation frequencies (Fig. 3c and Table 1).

The mechanical and electrical stimulation systems functioned properly as expected, with no contamination of the bioreactor culture occurring for 3 d. The morphology of the muscle tissues was examined after 3 d of culturing in the bioreactor under free-floating (Control), MS, or ES conditions. The gross morphology of the muscles in the Control group had a reduced CSA and overall length compared with that in the MS or ES group (Fig. S4 in the supplementary information), suggesting reduced atrophy in the stimulated muscles. This result was confirmed by H&E and Masson's trichrome staining of these muscles (Fig. 7a). Unstimulated muscles showed large, rounded myofibers, many of which lacked nuclei and contained vacuoles, indicating myofiber necrosis. The number of myofibers per field of view was significantly lower in the Control group than that in freshly excised muscles (Fresh) as well as in the MS and ES groups (Fig. 7b). The CSA of the myofiber in the Control group was also significantly larger than that in the Fresh, MS, and ES groups (Fig. 7c). The nucleus count per field of view (Fig. 7d) was significantly lower for all the other three experimental groups than the Fresh group, with the Control group having the lowest nucleus count. Similar to the case of CSA, the circumference of the Control group was significantly larger than that of the Fresh, MS, and ES groups (Fig. 7e). With the CSA and perimeter data, the circularity of the myofibers could be calculated using the formula $4\pi \times \text{CSA}/\text{perimeter}^2$. Myofibers from healthy skeletal muscle

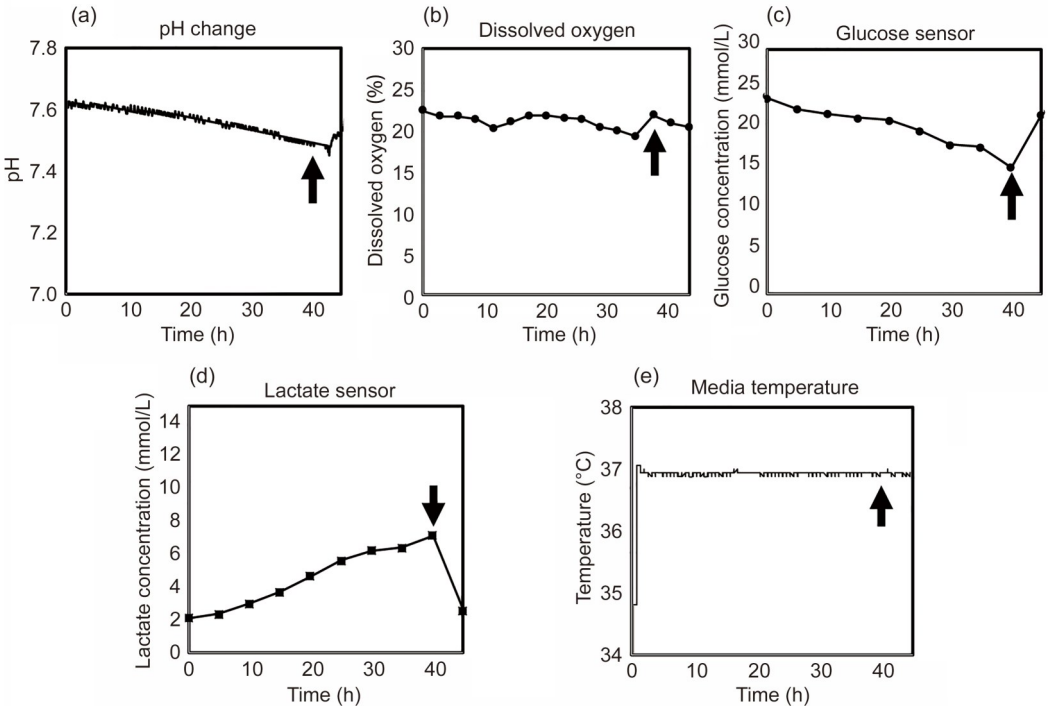

Fig. 6 Sensor loop system data with C2C12 cells cultured for 2 d. The cell culture plate's lid was modified to act as a bioreactor in the sensor loop system. pH (a), dissolved oxygen (b), glucose (c), lactate (d), and temperature (e) data were collected to observe changes during the culture. The arrows mark the media change

Table 1 Absolute force and average percentage peak force of the EDL muscle tested for contractile activity (n=5)

Stimulation (Hz)	Absolute force (gf)	Average percentage peak force (%)
1	1.16±1.06	15.5±14.10
20	3.10±2.13	32.1±7.80
30	6.33±2.13	59.9±12.80
60	9.72±7.71	92.8±7.30
100	9.82±7.39	96.2±5.70
140	7.33±5.01	75.3±10.90
160	5.91±3.07	68.7±22.30

EDL: extensor digitorum longus; gf: gram-force

tissues are polygonal, and necrotic myofibers become more rounded. Here, the data showed that the MS group better maintained the normal geometry of the myofiber compared to the Fresh group, whereas myofibers in the ES and Control groups were more rounded (Fig. 7f). These data suggested that mechanical stimulation might better preserve muscle tissue viability under the bioreactor culture conditions.

3.5 Bioreactor system validation with a tissue-engineered muscle construct

The ability of the bioreactor system to enhance the differentiation of tissue-engineered skeletal muscle constructs was also tested. After 14 d of culturing in the bioreactor system, the electrical and mechanical stimulation systems functioned normally without culture contamination. In addition, all engineered muscle samples in all experimental groups remained intact without any visible degradation.

All samples were evaluated macroscopically under a backlit light panel for comparison of translucence; a construct with higher optical density would suggest increased cell proliferation within the construct. In addition, an appropriately matured construct would be stiffer and show less sagging when held in a relaxed state under the same gravity field [56]. Here, the muscles from the ES group were more opaque under backlighting and shorter than those from the Control or MS group (Fig. 8a). Also, muscle tissue shrinkage and maturation after 14 d of culturing in differentiation media were comparable to those observed in previous studies [57, 58]. The diameter of the muscle in the ES group was smaller than that of the other groups (Fig. 8b). In addition, muscle constructs from both the MS and ES groups were stiffer than those from the Control group (Fig. 8c).

Morphologically, engineered muscles exposed to electrical stimulation had nuclei and elongated myotubes, indicating increased cell proliferation and differentiation (Fig. 9a). The muscle constructs from both the ES and MS groups had longer myotubes than those from the Control group (Fig. 9b), but the width of the myotubes in the ES group was thinner than that in other groups (Fig. 9c). These data

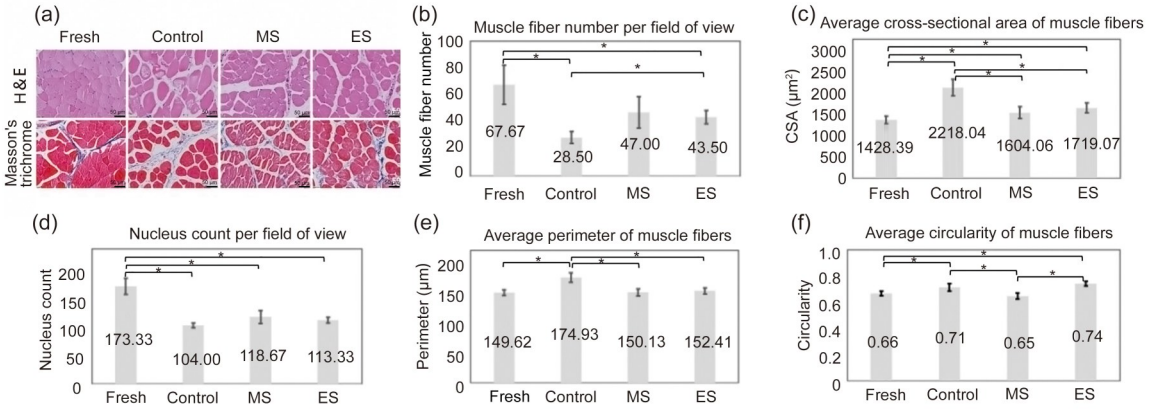

Fig. 7 Stimulation function validation tests with extensor digitorum longus muscle tissue after 3 d of culturing in the bioreactor. The histology results of the H&E and Masson's trichrome staining (a), muscle fibers per field of view (b), average CSA of muscle fibers (c), nucleus count per field of view at 20× (d), average perimeter of muscle fibers (e), and average circularity of muscle fibers (f) were compared for fresh tissue (Fresh) and three post-cultured groups, i.e., groups with mechanical stimulation (MS) and electrical stimulation (ES), and the static culturing group (Control). Data are expressed as mean±standard deviation; the sample number is n=3 for each group, $^{*}p$<0.05. H&E: hematoxylin and eosin; CSA: cross-sectional area

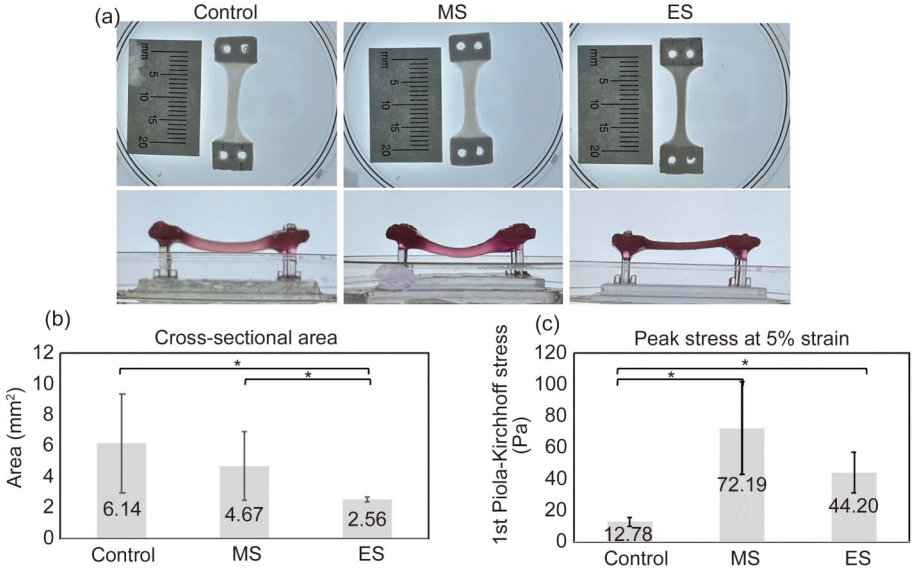

Fig. 8 Stimulation function validation tests with tissue-engineered muscle construct. (a) Representative images of the three culture groups post long-term bioreactor culture, i.e., the static culturing group (Control) and groups with mechanical stimulation (MS) and electrical stimulation (ES). (b) Quantification of the cross-sectional area using ImageJ. (c) Peak stress calculated from a 5% stretch for the Control, ES, and MS groups at the end of long-term culture. Data are expressed as mean±standard deviation; the sample number is n=3 for each group, $^{*}p$<0.05

suggest that the myotubes in the muscle constructs exposed to electrical stimulation had a thinner and more elongated morphology than those in the Control or MS group.

On the other hand, the nucleus number per myotube, or fusion index, may be determined using DAPI and myosin heavy chain (MHC) staining. The immunostaining result of samples stained with DAPI and MHC showed that both the ES and MS groups had significantly higher nucleus count per myotube than the Control group, with the ES group having the highest nucleus count (Fig. 9d). Likewise, the ES group had the highest fusion index compared to the other groups (Fig. 9e), suggesting that electrical stimulation might provide a better differentiation stimulus than mechanical stimulation, although both stimulation protocols resulted in a higher fusion index compared to the static control.

4 Discussion

The development of a novel uniaxial bioreactor was guided by the objective of creating a user-friendly and multifunctional system with high-throughput feedback capabilities for the long-term tissue culture, tissue maturation, and support

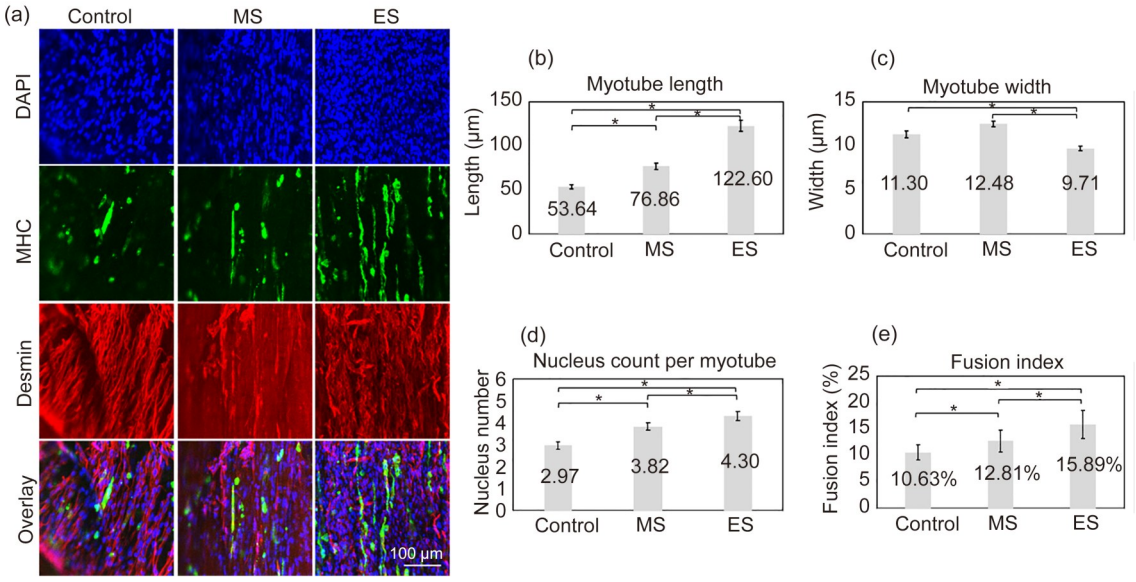

Fig. 9 Immunohistochemical image analysis for long-term culture. (a) DAPI, MHC, and desmin staining and overlay for cell proliferation and myotube formation observation in three culture groups, i.e., the static culturing group (Control) and groups with mechanical stimulation (MS) and electrical stimulation (ES). The overlay images represent for DAPI in blue color, MHC in green color, and desmin in red color. Quantification of myotube length (b), width (c), and nucleus count per myotube per field of view (d). (e) The number of nuclei fused to form myotubes as a percentage of the total number of nuclei per field of view was quantified. Data are expressed as mean±standard deviation; the sample number is n=3 for each group, $^{*}p<0.05$. DAPI: 4',6-diamidino-2-phenylindole; MHC: myosin heavy chain

of a functional cell phenotype. We achieved this by using a medical-grade photopolymer resin to design a leak-proof bioreactor chamber box assembly, into which the components and actuation elements could be snap-fit. This approach offers advantages, such as less time needed for fabricating new prototypes, accelerated implementation of new components, and efficient testing of strategies to enhance the overall structural integrity and utility of the bioreactor. While other bioreactors have been developed with materials such as polycarbonate [20], glass, plastics, or elastomers like acrylonitrile butadiene styrene (ABS) or polydimethylsiloxane (PDMS) [32], manufacturing processes using these materials are often costly, time-consuming, and have limited design flexibility. In contrast, additive manufacturing allows for the production of specifically designed components that would otherwise be challenging to manufacture. Future improvements could include using 3D-printed actuation elements made from stainless steel or more durable resin, which would increase the performance and strength of the moving parts. Lastly, a total of three tissue samples can be simultaneously cultured dynamically with or without other sensors described in this paper. Due to the volume capacity of the 3D printer utilized in this study, we decided on a three-lane system.

Regarding mechanical stimulation, this bioreactor system features independent cycle programming, parametric strain protocol definition, software handling of microstepping, and encoder feedback, enabling precise control and customization of the mechanical stimulation. For our study, we opted not to use sine waves for strain cycles to keep the strain rates constant [59], although our system is compatible with this approach. Commercially available systems [60] are costly and limited in the types of tissue geometry and scaffolding biomaterials that they can accommodate.

The integration of a force sensor into the system enabled the measurement of the contractile force (Fig. 3c), the non-destructive quantification of the mechanical properties (Fig. 3e), and the force feedback during the dynamic strain conditioning (Fig. S5 and Video S3 in the supplementary information). Two experiments were performed to validate the functionality of the force sensor. First, the rat EDL muscle tissue was used to determine the isometric twitch and tetanic contractile forces at different frequencies of electrical stimulation. The force output during the stretch, the 3D morphology of the cross-sectional areas over time, and the applied strain were determined at each time point for a more comprehensive mechanical property characterization. In the second validation experiment, the material properties of the cellular and acellular engineered muscle scaffolds were characterized, and the peak forces were measured from the force feedback of strain cycles of different maximum strain percentages. In addition, including a force measurement system expanded the capabilities of the bioreactor to measure the forces exerted by the tissue during mechanical or electrical stimulation, providing valuable insights into tissue differentiation and maturation. Using freshly excised EDL muscles, the system's functionality upon fixed voltage field stimulation and force measurements of contractile

responses was verified, and the contractile responses in five muscle samples tested showed moderate variability relative to muscle volume. However, the overall trend with increasing frequencies showed a pattern of response similar to those previously reported [37, 61, 62].

In addition, to determine the functionality of tissue-engineered muscle constructs, force sensing can be utilized for testing in situ scaffolds by combining it with a stepper motor program to generate force–displacement curves. These data, along with information on tissue geometry, can be used to calculate the stress–strain/stiffness curve for the wet testing of mechanical properties [63]. Also, force sensing helps resolve the issue of achieving uniform pretension loading of the scaffolds. This is done by monitoring the force generation curves with a small incremental strain, starting from a zero-force sagging position and moving the tissue holder away while measuring the force [20]. Having a readout of the stretching force in real time can provide information on changes in the material properties of the construct after many stretch cycles. Force sensors within the bioreactor can also assist in the comparison of an engineered construct with native tissue, such as freshly excised muscles.

Additionally, an essential aspect of the pretensioning system is relevant to both the dynamic [20] and isometric force testing [61] of muscle tissues. Researchers have used a system for adjusting the initial length or initial tension for each muscle sample, where the tissue constructs must be placed in the bioreactor to extend to their greatest lengths without being stretched. The development of these pretensioning systems arose due to the challenge of having a single motor to actuate multiple tissues. Here, we have implemented a simple "pretensioning" system directly into our system by independent software control of the motors for each lane. A desired pretensioning length was achieved non-invasively by commanding each idle motor to step back or forward a given length to adjust the tension prior to the acquisition of force measurements (Fig. 3). For testing the material properties with or without cells, the motor was programmed to stop at a specific time before the next step, considering the stress relaxation. Due to the incorporated microstepping, we could accurately define small stretching steps of 0.5% in 0.1 s for mechanical testing without motor artifacts interfering with force sensor readings, which was an issue in other studies [63]. Finally, taking our engineered muscle casting method into account, the known initial CSA of the muscle construct and real-time stepping information within the code can be used to directly generate output stress–strain curves in real time.

Here, the validation tests have demonstrated that this system can read forces accurately across wide ranges, can be fine-tuned or calibrated for specific use cases, and can be saved for end use in the reprogrammable read-only memory. Previously, the direct sensing of the contractile force was achieved using in-line [64] and bending beam force sensors [20] with very high sensitivity [65]. Since tissue sizes may vary depending on the user application, a sensor with high corrosion and water resistance and reliable measurements over wide ranges was developed. Here, we have successfully demonstrated how the incorporated force sensors can be utilized for different purposes (Fig. 3 and Fig. S5 in the supplementary information). The force-sensing capability of our bioreactor can also be used to program an alarm system, which will be activated if the tissue is detached from the holder or becomes misaligned, as indicated by no or significantly lower change in force when the same strain is re-applied in subsequent cycles. This functionality can provide an additional safeguard for timely intervention if any issues are detected during the experiment. In the future, a more sensitive micronewton force sensor can be easily incorporated to gather cell-level force data.

An electrical stimulator was incorporated into the bioreactor system by considering factors such as electrode material and geometry to develop a non-cytotoxic, non-corrosive, and sterilizable system that would produce a straight field stimulus generated over the desired fluid volume. The detachable electrode holders designed for the device could be easily reconfigured to adjust the shape of the field. Given the importance of maintaining a uniform electric field throughout the tissue, integrated plate electrodes were used instead of rod or point electrodes, ensuring a uniform unidirectional field distribution and supporting a more uniform and consistent electrical stimulation across the tissue. It is important to maintain a uniform electric field for testing contractile activity and development of the stimulated tissue [66–68]. Further, in-phase or out-of-phase electrical and mechanical co-stimulation studies [55] can be easily performed in this system, as the initiation of the electrical pulse can be triggered before, during, or after the corresponding mechanical cycle. A variety of strain protocols combining the two stimuli can be generated.

Monitoring the physiological conditions within the tissue culture is critical [69–71]. DO, pH, glucose, lactate, and temperature sensors provide real-time data on the essential parameters that influence the structure and functionality of a maturing tissue construct. Here, the reliability of the repeated measurements in this system was demonstrated by performing peak matching. As a result, the slight timestamp drift when using a low-frequency microcontroller for long-term continuous testing can be avoided. Our data indicate that our sampling system reliably automated the correct fluid routing to the sensors (Fig. S1 in the supplementary information). Sensor degradation over time was expected for the glucose-and-lactate oxidase-based sensors due to the reactions that generate the output current. The 72 sampling cycles presented in the results showed negligible changes in the readings from the calibration solution, confirming that

the sensor system could be used for more extended culturing using independent re-calibration.

Finally, the sensor loop system displayed stable and significant readings in the small-volume experiments using C2C12 cells, validating the functionality of the bioreactor for cell manufacturing (Fig. 6). The sensor loop system described in this study will enhance the repeatability and reliability of the experimental results in translational research and contribute to the automation of quality control in clinical manufacturing.

Regular media exchange has always been a challenge for the long-term culturing of cells and tissues. Laboratory and commercial media exchange systems typically use two pumps for small [72] and large [73] culture volumes, respectively (AMX, Agilent Biotek, Winooski, VT, USA). Our system was designed to maintain a constant culture media volume by utilizing a commercially available single-channel stepper motor-based peristaltic pump with a multifunctional driver board. This setup provides easy control of the pump speed, frequent flow rate calibrations, and easy integration with the larger bioreactor system. Additionally, threshold sensor outputs can be programmed to trigger media exchanges automatically. The pump driving the sensor loop and the media exchanger in our system are panel-mounted, reducing the device footprint. The commercial media exchange systems designed for research laboratory use are generally much more costly than the system we have developed.

Rat EDL muscles were used to validate both mechanical and electrical conditioning within the bioreactor. Although the excised muscle degraded rapidly, histological analysis indicated that tissue morphology was maintained for 3 d of bioreactor culturing (Fig. 7). Skeletal muscle explants for ex vivo studies have been used to elucidate muscle anatomy, physiology, and function [74]. It is challenging to keep excised muscles viable in a long-term culture because of limiting factors, such as a lack of active perfusion through the supporting vasculature [74, 75]. Muscle degradation can be slowed down, as evidenced by the better-maintained muscle morphology in the MS or ES group compared with the Control group in our EDL explant viability study. However, degradation during the ex vivo culture of the muscle explant was still inevitable owing to its dense, compact structure and the lack of the original intact vasculature for active perfusion. This finding demonstrates the ability of the bioreactor system to preserve normal tissue structure and prevent degradation by applying electrical or mechanical stimulation, or both.

The bioreactor system was also validated for its ability to stimulate the differentiation and maturation of skeletal muscle tissue constructs over 14 d. C2C12 cells differentiate and form myotubes when they have been cultured for 10–14 d [29, 76–82]. Here, myogenic C2C12 cells were embedded in fibrin and cast into a mold [29, 43, 46, 55, 77, 81, 83–86]. The stimulated constructs demonstrated increased myotube formation compared with the Control group (Fig. 9); this finding was similar to the results of other research groups. For example, Aguilar-Agon et al. cultured engineered muscle for 14 d, followed by 15% mechanical stimulation, and reported that mechanical stimulation induced hypertrophy and improved the force production of the engineered muscle with evidence of wider myotubes, more nuclei per myotube, and a higher fusion index [29]. Another study [80] applied 10% static or dynamic strain during differentiation for 7 d and concluded that myotube maturation increased in the mechanically stimulated group, as evidenced by an increase in myotube-associated nuclei and larger myotube diameter compared with the unstimulated controls. According to Khodabukus et al., electrical stimulation promoted human muscle hypertrophy, structural organization, myotube maturation, force generation, and metabolic flux when applied from Day 7 to Day 14 during differentiation [82]. Under electrical stimulation, the experimental group showed increased formation of myotubes that were longer and wider than those in the Control group; these effects were further enhanced in the field created by the circular electrodes compared to the parallel electrodes [83]. The difference in sagging of constructs in different groups pointed to the difference in their post-culture length, which was another important aspect to consider when using stretched versus non-stretched fibrin gel constructs (Fig. 8a). The ES group displayed the least change in myotube length and could be a better choice for avoiding plastic deformations in tissue length [57].

Therefore, our novel uniaxial bioreactor has demonstrated tremendous potential for conditioning engineered muscle tissues. Compared to previously developed bioreactors for this purpose, we have integrated mechanical, electrical, and sensor capabilities to offer researchers a versatile tool for investigating cellular responses, tissue development, and contractile activity under controlled stimulations. In terms of scaling up and developing throughput capabilities in the future, this size of design can be easily upgraded in terms of the size of the motors to provide larger torque or a greater number of lanes, as needed for the target tissue product's manufacturing purposes.

Overall, this system has undergone rigorous qualification processes, ensuring its robustness and reliability. However, the currently developed prototypes have some limitations. Due to the complexity of the design, more time is needed to pre-clean and dry the 3D-printed parts and mate them together than in traditional methods. This process does not affect the tissue loading time, as the culture box is prepared with motor, encoder, and force sensor wires ending with connectors in one bag (lid separate) that are sterilized together at low-temperature ethylene oxide. It takes one

person to assemble the culture box tray with constructs in a total of less than 15 min, including rinsing with PBS, anchoring the constructs, filling with media, closing the lid, and transferring to the incubator as a complete tray. One can then assemble the sensor tray, which takes another 10 min in the hood. The operation can start once the wires coming out of the incubator are connected to their respective ports. For future development, we plan to combine the wiring in an easy-to-apply multipin connector that makes multicomponent connection easy and quick.

Another issue is that the developed media sensing system did not capture the changes in long-term culturing due to the high volume of the combined media. This issue was addressed using 2D culture to demonstrate the system's functionality to sense or manipulate the combined environment of the three tissue samples. Similar to previously developed tissue beds [20], the future iteration of the bioreactor can have separate media channels per tissue sample, and the described media sensing system can be programmed to capture fluids intermittently from each lane, one by one.

Other commercial bioreactors, such as those from FlexCell® and StrexCell®, can stretch the scaffold in 1D or 2D precisely but lack some of the advanced monitoring or analysis capability integrated within our system. The utilization of 3D printing technology, leak-proof assembly, customizable mechanical and electrical stimulation, force-sensing capabilities, sensor loops, and advanced features in the measurement systems make this novel uniaxial bioreactor an asset for tissue engineering and biomedical research.

Additionally, this design can serve as the foundation for other types of complex tissue engineering bioreactors with improved feedback and a higher degree of automation, which can be rapidly developed and prototyped. The incubated mounting tray system, perfusion port design, and environment monitoring and maintenance system have utilities beyond uniaxial tissue culture. The culture box can fit in other base plates, as used by the force sensor assembly, to modify the internal tissue anchoring system without the need for another box. This system can also support long-term biological experiments and offer hands-free operations that can be managed through a computer without disturbing the incubation or sterility of tissue samples. All these features are critical for tissue maturation regardless of its type. Moreover, the stimulation programs can be updated in real time either manually or through sensor feedback. This is a critical step in making the experiments more quality-controlled, repeatable, and translatable to fully autonomous culture systems.

5 Conclusions

The development of a multifunctional bioreactor with two types of integrated stimulation systems and feedback from physical and biological sensing enables the execution of conditioning protocols to enhance the consistency, functionality, and durability of the engineered skeletal muscle. The components and production methods used to develop this bioreactor can be easily adapted for other tissue applications that can benefit from unidirectional stimulation to fully mature multiple constructs or large volumetric tissues. The feedback obtained from this device on the tissue maturation status, along with the ability to take real-time in situ measurements that indicate tissue differentiation, maturation, and growth, provides new manufacturing strategies to advance the field of tissue engineering to clinical applications.

Supplementary Information The online version contains supplementary material available at https://doi.org/10.1631/bdm.2400235.

Acknowledgements The authors would like to thank our industry collaborators as well as the Wake Forest Institute for Regenerative Medicine for the bioreactor research program. Funding was made possible by the US Army Medical Research and Development Command through the Medical Technology Enterprise Consortium under Contract #W81XWH-15-9-0001.

Author contributions Bioreactor design and manuscript writing: AM and PFL; review & editing: ER, TC, TDS, JHK, AA, FCM, MNG, SS, JH, JJY, and YMJ.

Declarations

Conflict of interest JJY is an editorial board member for *Bio-Design and Manufacturing* and was not involved in the editorial review or the decision to publish this article. The authors declare that they have no conflict of interest.

Ethical approval The EDL tissue specimens were collected from the rats euthanized under an existing Wake Forest University Institutional Animal Care and Use Committee (IACUC) approved protocol (A20-147).

Disclaimer The views and conclusions contained herein are those of the authors and should not be interpreted as necessarily representing the official policies or endorsements, either expressed or implied, by the U.S. Government.

References

1. Schaechter M (2009) Encyclopedia of Microbiology (3rd Ed.). Elsevier/Academic Press, Tokyo. https://doi.org/10.1016/B978-012373944-5
2. Partap S, Plunkett NA, O'brien FJ (2010) Bioreactors in tissue engineering. In: Daniel E (Ed.), Tissue Engineering. IntechOpen, p.323–337. https://doi.org/10.5772/8579
3. Antoni D, Burckel H, Josset E et al (2015) Three-dimensional cell culture: a breakthrough in vivo. Int J Mol Sci 16(3):5517–5527. https://doi.org/10.3390/ijms16035517
4. Martin I, Wendt D, Heberer M (2004) The role of bioreactors in tissue engineering. Trends Biotechnol 22(2):80–86. https://doi.org/10.1016/j.tibtech.2003.12.001
5. Grayson WL, Martens TP, Eng GM et al (2009) Biomimetic

approach to tissue engineering. Semin Cell Dev Biol 20(6):665–673.
https://doi.org/10.1016/j.semcdb.2008.12.008
6. Bertucci C, Koppes R, Dumont C (2019) Neural responses to electrical stimulation in 2D and 3D in vitro environments. Brain Res Bull 152:265–284.
https://doi.org/10.1016/j.brainresbull.2019.07.016
7. Castro N, Ribeiro SO, Fernandes MM et al (2020) Physically active bioreactors for tissue engineering applications. Adv Biosyst 4(10):e2000125.
https://doi.org/10.1002/adbi.202000125
8. Rangarajan S, Madden L, Bursac N (2014) Use of flow, electrical, and mechanical stimulation to promote engineering of striated muscles. Ann Biomed Eng 42(7):1391–1405.
https://doi.org/10.1007/s10439-013-0966-4
9. Ravichandran, A, Liu YC, Teoh SH (2018) Bioreactor design towards generation of relevant engineered tissues: focus on clinical translation. J Tissue Eng Regener Med 12(1):e7–e22.
https://doi.org/10.1002/term.2270
10. Lim D, Renteria ES, Sime DS et al (2022) Bioreactor design and validation for manufacturing strategies in tissue engineering. Bio-Des Manuf 5(1):43–63.
https://doi.org/10.1007/s42242-021-00154-3
11. Massai D, Meglio FD, Serino G et al (2019) Application of 3D printing technology for design and manufacturing of customized components for a mechanical stretching bioreactor. J Healthc Eng 2019(1):3957931.
https://doi.org/10.1155/2019/3957931
12. Carbonaro D, Putame G, Castaldo C et al (2020) A low-cost scalable 3D-printed sample-holder for agitation-based decellularization of biological tissues. Med Eng Phys 85:7–15.
https://doi.org/10.1016/j.medengphy.2020.09.006
13. Musgrove HB, Catterton MA, Pompano RR (2022) Applied tutorial for the design and fabrication of biomicrofluidic devices by resin 3D printing. Anal Chim Acta 1209:339842.
https://doi.org/10.1016/j.aca.2022.339842
14. Bayarsaikhan E, Lim JH, Shin SH et al (2021) Effects of postcuring temperature on the mechanical properties and biocompatibility of three-dimensional printed dental resin material. Polymers 13(8):1180.
https://doi.org/10.3390/polym13081180
15. Jeršovaitė J, Šarachovaitė U, Matulaitienė I et al (2023) Biocompatibility enhancement via post-processing of microporous scaffolds made by optical 3D printer. Front Bioeng Biotechnol 11: 1167753.
https://doi.org/10.3389/fbioe.2023.1167753
16. Abousleiman RI, Sikavitsas VI (2006) Bioreactors for tissues of the musculoskeletal system. Adv Exp Med Biol 585:243–259.
https://doi.org/10.1007/978-0-387-34133-0_17
17. Frontera WR, Ochala J (2015) Skeletal muscle: a brief review of structure and function. Calcif Tissue Int 96:183–195.
https://doi.org/10.1007/s00223-014-9915-y
18. Smoak MM, Mikos AG (2020) Advances in biomaterials for skeletal muscle engineering and obstacles still to overcome. Mater Today Bio 7:100069.
https://doi.org/10.1016/j.mtbio.2020.100069
19. Heher P, Maleiner B, Prüller J et al (2015) A novel bioreactor for the generation of highly aligned 3D skeletal muscle-like constructs through orientation of fibrin via application of static strain. Acta Biomater 24:251–265.
https://doi.org/10.1016/j.actbio.2015.06.033
20. Cook CA, Huri PY, Ginn BP et al (2016) Characterization of a novel bioreactor system for 3D cellular mechanobiology studies. Biotechnol Bioeng 113(8):1825–1837.
https://doi.org/10.1002/bit.25946
21. Mantero S, Sadr N, Riboldi SA et al (2007) A new electromechanical bioreactor for soft tissue engineering. J Appl Biomater Biomech 5(2):107–116.
22. Powell CA, Smiley BL, Mills J et al (2002) Mechanical stimulation improves tissue-engineered human skeletal muscle. Am J Physiol Cell Physiol 283(5):C1557–C1565.
https://doi.org/10.1152/ajpcell.00595.2001
23. Chang YJ, Chen YJ, Huang CW et al (2016) Cyclic stretch facilitates myogenesis in C2C12 myoblasts and rescues thiazolidinedione-inhibited myotube formation. Front Bioeng Biotechnol 4:27.
https://doi.org/10.3389/fbioe.2016.00027
24. Pisanu A, Reid G, Fusco D et al (2022) Bizonal cardiac engineered tissues with differential maturation features in a mid-throughput multimodal bioreactor. iScience 25(5):104297.
https://doi.org/10.1016/j.isci.2022.104297
25. Putame G, Gabetti S, Carbonaro D et al (2020) Compact and tunable stretch bioreactor advancing tissue engineering implementation. Application to engineered cardiac constructs. Med Eng Phys 84:1–9.
https://doi.org/10.1016/j.medengphy.2020.07.018
26. Pang QM, Zu JW, Siu GM et al (2010) Design and development of a novel biostretch apparatus for tissue engineering. J Biomech Eng 132(1):014503.
https://doi.org/10.1115/1.3005154
27. Wu MH, Wang HY, Liu HL et al (2011) Development of high-throughput perfusion-based microbioreactor platform capable of providing tunable dynamic tensile loading to cells and its application for the study of bovine articular chondrocytes. Biomed Microdev 13(4):789–798.
https://doi.org/10.1007/s10544-011-9549-z
28. Cole K, Henano N, Miller T et al (2015) Mechanical and Electrical Stimulation Device for the Creation of a Functional Unit of Human Skeletal Muscle In Vitro. Worcester Polytechnic Institute, Worcester, MA, USA, Project No. RLP-1401
29. Aguilar-Agon KW, Capel AJ, Martin NRW et al (2019) Mechanical loading stimulates hypertrophy in tissue-engineered skeletal muscle: molecular and phenotypic responses. J Cell Physiol 234(12):23547–23558.
https://doi.org/10.1002/jcp.28923
30. Wang T, Gardiner BS, Lin Z et al (2013) Bioreactor design for tendon/ligament engineering. Tissue Eng Part B Rev 19(2):133–146.
https://doi.org/10.1089/ten.TEB.2012.0295
31. Chen ZM, Chen PL, Ruan R et al (2020) Applying a three-dimensional uniaxial mechanical stimulation bioreactor system to induce tenogenic differentiation of tendon-derived stem cells. J Vis Exp 2020(162):e61278.
https://doi.org/10.3791/61278
32. Béland J, Duverger JE, Petitjean E et al (2020). Development of an open hardware bioreactor for optimized cardiac cell culture integrating programmable mechanical and electrical stimulations. AIP Adv 10(3):035133.
https://doi.org/10.1063/1.5144922
33. Donnelly K, Alastair K, Andrew P et al (2010) A novel bioreactor for stimulating skeletal muscle in vitro. Tissue Eng Part C Methods 16(4):711–718.
https://doi.org/10.1089/ten.tec.2009.0125
34. Zheng XS, Tan C, Castagnola E et al (2021) Electrode materials for chronic electrical microstimulation. Adv Healthc Mater 10(12): e2100119.
https://doi.org/10.1002/adhm.202100119
35. Tandon N, Cannizzaro C, Chao PHG et al (2009) Electrical stimulation systems for cardiac tissue engineering. Nat Protoc 4(2):155–173.
https://doi.org/10.1038/nprot.2008.183

36. Mobini S, Leppik L, Parameswaran TV et al (2017) In vitro effect of direct current electrical stimulation on rat mesenchymal stem cells. PeerJ 5:e2821. https://doi.org/10.7717/peerj.2821
37. Park KH, BrottoL, Lehoang O et al (2012) Ex vivo assessment of contractility, fatigability and alternans in isolated skeletal muscles. J Vis Exp 69:e4198. https://doi.org/10.3791/4198
38. Dennis RG, Kosnik PE (2000) Excitability and isometric contractile properties of mammalian skeletal muscle constructs engineered in vitro. In Vitro Cell Dev Biol Anim 36(5):327–335. https://doi.org/10.1290/1071-2690(2000)036<0327:EAICPO>2.0.CO;2
39. Morgan KY, Black LD (2014) Mimicking isovolumic contraction with combined electromechanical stimulation improves the development of engineered cardiac constructs. Tissue Eng Part A 20(11-12):1654–1667. https://doi.org/10.1089/ten.TEA.2013.0355
40. Gilbert-Honick J (2020). Engineering Skeletal Muscle for Histological and Functional Regeneration Following Volumetric Muscle Loss. Doctoral Dissertation, Johns Hopkins University, USA
41. Khodabukus A, Baar K (2012) Defined electrical stimulation emphasizing excitability for the development and testing of engineered skeletal muscle. Tissue Eng Part C Methods 18(5): 349–357. https://doi.org/10.1089/ten.TEC.2011.0364
42. McMahon DK, Anderson PA, Nassar R et al (1994) C2C12 cells: biophysical, biochemical, and immunocytochemical properties. Am J Physiol 266(6 Pt 1):C1795–C1802. https://doi.org/10.1152/ajpcell.1994.266.6.C1795
43. Hofemeier AD, Limon T, Muenker TM et al (2021) Global and local tension measurements in biomimetic skeletal muscle tissues reveals early mechanical homeostasis. eLife 10:e60145. https://doi.org/10.7554/eLife.60145
44. Yoshioka K, Ito A, Arifuzzaman M et al (2021) Miniaturized skeletal muscle tissue fabrication for measuring contractile activity. J Biosci Bioeng 131(4):434–441. https://doi.org/10.1016/j.jbiosc.2020.11.014
45. Wang BW, Wang ZW, Chen T et al (2020) Development of novel bioreactor control systems based on smart sensors and actuators. Front Bioeng Biotechnol 8:7. https://doi.org/10.3389/fbioe.2020.00007
46. Akiyama Y, Nakayama A, Nakano S et al (2021) An electrical stimulation culture system for daily maintenance-free muscle tissue production. Cyborg Bionic Syst 2021:9820505. https://doi.org/10.34133/2021/9820505
47. Wheatley BB, Morrow DA, Odegard GM et al (2016) Skeletal muscle tensile strain dependence: hyperviscoelastic nonlinearity. J Mechan Behav Biomed Mater 53:445–454. https://doi.org/10.1016/j.jmbbm.2015.08.041
48. Čorović S, Pavlin M, Miklavčič D (2007) Analytical and numerical quantification and comparison of the local electric field in the tissue for different electrode configurations. BioMed Eng OnLine 6:37. https://doi.org/10.1186/1475-925X-6-37
49. Gabetti S, Sileo A, Montrone F et al (2023) Versatile electrical stimulator for cardiac tissue engineering—investigation of charge-balanced monophasic and biphasic electrical stimulations. Front Bioeng Biotechnol 10:1031183. https://doi.org/10.3389/fbioe.2022.1031183
50. Prill S, Jaeger MS, Duschl C (2014) Long-term microfluidic glucose and lactate monitoring in hepatic cell culture. Biomicrofluidics 8(3):034102. https://doi.org/10.1063/1.4876639
51. Somers SM, Spector AA, DiGirolamo DJ et al (2017) Biophysical stimulation for engineering functional skeletal muscle. Tissue Eng Part B Rev 23(4):362–372. https://doi.org/10.1089/ten.TEB.2016.0444
52. Pennisi CP, Olesen CG, Zee M et al (2011) Uniaxial cyclic strain drives assembly and differentiation of skeletal myocytes. Tissue Eng Part A 17(19-20):2543–2550. https://doi.org/10.1089/ten.TEA.2011.0089
53. Tandon N, C Cannizzaro, Figallo E et al (2006) Characterization of electrical stimulation electrodes for cardiac tissue engineering. In: International Conference of the IEEE Engineering in Medicine and Biology Society, p.845–848. https://doi.org/10.1109/IEMBS.2006.259747
54. Cannizzaro C, Tandon N, Figallo E et al (2007) Practical aspects of cardiac tissue engineering with electrical stimulation. Methods Mol Med 140:291–307. https://doi.org/10.1007/978-1-59745-443-8_16
55. Kim H, Kim MC, Asada HH (2019) Extracellular matrix remodelling induced by alternating electrical and mechanical stimulations increases the contraction of engineered skeletal muscle tissues. Sci Rep 9(1):2732. https://doi.org/10.1038/s41598-019-39522-6
56. Guimarães CF, Gasperini L, Marques AP et al (2020) The stiffness of living tissues and its implications for tissue engineering. Nat Rev Mater 5(5):351–370. https://doi.org/10.1038/s41578-019-0169-1
57. Turner DC, Kasper AM, Seaborne RA et al (2019) Exercising bioengineered skeletal muscle in vitro: biopsy to bioreactor. Methods Mol Biol 1889:55–79. https://doi.org/10.1007/978-1-4939-8897-6_5
58. Roberts IV, Donno R, Galli F et al (2022) The contracture-in-a-well. An in vitro model distinguishes bulk and interfacial processes of irreversible (fibrotic) cell-mediated contraction. Biomater Adv 133:112661. https://doi.org/10.1016/j.msec.2022.112661
59. Ouyang XL, Xie YF, Wang GH (2019) Mechanical stimulation promotes the proliferation and the cartilage phenotype of mesenchymal stem cells and chondrocytes co-cultured in vitro. Biomed Pharmacother 117:109146. https://doi.org/10.1016/j.biopha.2019.109146
60. Fonseca FRM, Carvalho ÓSN, Gasik M et al (2023) Mechanical stimulation devices for mechanobiology studies: a market, literature, and patents review. Bio-Des Manuf 6(3):340–371. https://doi.org/10.1007/s42242-023-00232-8
61. Vallejo J, Spence M, Cheng AL et al (2016) Cellular and physiological effects of dietary supplementation with β-hydroxy-β-methylbutyrate (HMB) and β-alanine in late middle-aged mice. PLoS ONE 11(3):e0150066. https://doi.org/10.1371/journal.pone.0150066
62. Chan S, Head SI (2010) Age-and gender-related changes in contractile properties of non-atrophied EDL muscle. PLoS ONE 5(8):e12345. https://doi.org/10.1371/journal.pone.0012345
63. Somers SM, Grayson WL (2021) Protocol for the use of a novel bioreactor system for hydrated mechanical testing, strained sterile culture, and force of contraction measurement of tissue engineered muscle constructs. Front Cell Dev Biol 9:661036. https://doi.org/10.3389/fcell.2021.661036
64. Meinert C, Schrobback K, Hutmacher DW et al (2017) A novel bioreactor system for biaxial mechanical loading enhances the properties of tissue-engineered human cartilage. Sci Rep 7(1): 16997. https://doi.org/10.1038/s41598-017-16523-x
65. Rizzuto E, Carosio S, Faraldi M et al (2016) A DIC based technique to measure the contraction of a skeletal muscle engineered

tissue. Appl Bionics Biomech 2016:7465095. https://doi.org/10.1155/2016/7465095
66. Tsai HF, Cheng JY, Chang HF et al (2016) Uniform electric field generation in circular multi-well culture plates using polymeric inserts. Sci Rep 6(1):26222. https://doi.org/10.1038/srep26222
67. Chen C, Bai X, Ding YH et al (2019) Electrical stimulation as a novel tool for regulating cell behavior in tissue engineering. Biomater Res 23:25. https://doi.org/10.1186/s40824-019-0176-8
68. Meng SY, Rouabhia M, Zhang Z (2021) Electrical stimulation and cellular behaviors in electric field in biomedical research. Materials 15(1):165. https://doi.org/10.3390/ma15010165
69. Reardon KF (2021) Practical monitoring technologies for cells and substrates in biomanufacturing. Curr Opin Biotechnol 71: 225–230. https://doi.org/10.1016/j.copbio.2021.08.006
70. Ferrari E, Palma C, Vesentini S et al (2020) Integrating biosensors in organs-on-chip devices: a perspective on current strategies to monitor microphysiological systems. Biosensors 10(9): 110. https://doi.org/10.3390/bios10090110
71. Kieninger J, Weltin A, Flamm H et al (2018) Microsensor systems for cell metabolism–from 2D culture to organ-on-chip. Lab Chip 18(9):1274–1291. https://doi.org/10.1039/c7lc00942a
72. Koike H, Kubota K, Sekine K et al (2012) Establishment of automated culture system for murine induced pluripotent stem cells. BMC Biotechnol 12(1):81. https://doi.org/10.1186/1472-6750-12-81
73. Lovecchio J, Gargiulo P, Vargas Luna JL et al (2019) A standalone bioreactor system to deliver compressive load under perfusion flow to hBMSC-seeded 3D chitosan-graphene templates. Sci Rep 9(1):16854. https://doi.org/10.1038/s41598-019-53319-7
74. Smith LR, Meyer GA (2020) Skeletal muscle explants: ex-vivo models to study cellular behavior in a complex tissue environment. Connect Tissue Res 61(3-4):248–261. https://doi.org/10.1080/03008207.2019.1662409
75. Leijendekker W, Elzinga G (1990) Metabolic recovery of mouse extensor digitorum longus and soleus muscle. Pflügers Archiv 416(1-2):22–27. https://doi.org/10.1007/BF00370217
76. Nagashima T, Hadiwidjaja S, Ohsumi S et al (2020) In vitro model of human skeletal muscle tissues with contractility fabricated by immortalized human myogenic cells. Adv Biosyst 4(11): e2000121. https://doi.org/10.1002/adbi.202000121
77. Grant L, Raman R, Cvetkovic C et al (2019) Long-term cryopreservation and revival of tissue-engineered skeletal muscle. Tissue Eng Part A 25(13-14):1023–1036. https://doi.org/10.1089/ten.tea.2018.0202
78. Shimizu K, Ohsumi S, Kishida T et al (2020) Fabrication of contractile skeletal muscle tissues using directly converted myoblasts from human fibroblasts. J Biosci Bioeng 129(5):632–637. https://doi.org/10.1016/j.jbiosc.2019.11.013
79. Fleming JW, Capel AJ, Rimington RP et al (2020) Bioengineered human skeletal muscle capable of functional regeneration. BMC Biol 18(1):145. https://doi.org/10.1186/s12915-020-00884-3
80. Somers SM, Zhang NY, Morrissette-McAlmon JBF et al (2019) Myoblast maturity on aligned microfiber bundles at the onset of strain application impacts myogenic outcomes. Acta Biomater 94:232–242. https://doi.org/10.1016/j.actbio.2019.06.024
81. Wragg NM, Player DJ, Martin NRW et al (2019) Development of tissue-engineered skeletal muscle manufacturing variables. Biotechnol Bioeng 116(9):2364–2376. https://doi.org/10.1002/bit.27074
82. Khodabukus A, Madden L, Prabhu NK et al (2019) Electrical stimulation increases hypertrophy and metabolic flux in tissue-engineered human skeletal muscle. Biomaterials 198:259–269. https://doi.org/10.1016/j.biomaterials.2018.08.058
83. Liu LQ, Zhang C, Wang WX et al (2018) Regulation of C2C12 differentiation and control of the beating dynamics of contractile cells for a muscle-driven biosyncretic crawler by electrical stimulation. Soft Robot 5(6):748–760. https://doi.org/10.1089/soro.2018.0017
84. Shimizu K, Genma R, Gotou Y et al (2017) Three-dimensional culture model of skeletal muscle tissue with atrophy induced by dexamethasone. Bioengineering 4(2):56. https://doi.org/10.3390/bioengineering4020056
85. Fleming JW, Capel AJ, Rimington RP et al (2019) Functional regeneration of tissue engineered skeletal muscle in vitro is dependent on the inclusion of basement membrane proteins. Cytoskeleton 76(6):371–382. https://doi.org/10.1002/cm.21553
86. Jones MG, Andriotis OG, Roberts JJW et al (2018) Nanoscale dysregulation of collagen structure-function disrupts mechano-homeostasis and mediates pulmonary fibrosis. eLife 7:e36354. https://doi.org/10.7554/eLife.36354